Chapter 6

Deconvolution of wide field images

"You can have anything you want,
- if you want it badly enough.
You can be anything you want to,
do anything you set out to accomplish,
- if you hold to that desire with singleness of purpose."
- Abraham Lincoln

In this chapter, we discuss the deconvolution of the full resolution wide field dirty images. Due to non-coplanarity, the Point Spread Function (PSF) becomes declination dependent. This difficulty is further compounded by the declination dependence of the bandwidth decorrelation and natural stretching of the FWHM of the beam in RA by $\sec(\delta)$. We present the algorithm developed for deconvolving wide field images made using the non-coplanar MRT, with a varying PSF. Important aspects of the applied procedure are described and the results are presented in form of deconvolved images. We start with a brief introduction and review of the earlier work carried out related to deconvolution of MRT images.

6.1 Introduction

A dirty image obtained by Fourier inversion of the sampled visibilities is the convolution of brightness distribution of the sky with the synthesized beam or the Point Spread Function of the array. This is represented by,

$$I^D(l,m) = I^t(l,m) * P(l,m,n) \tag{6.1}$$

where $I^D(l,m)$ is the dirty image, $I^t(l,m)$ is the true brightness distribution of the sky and $P(l,m,n)$ is the synthesized beam or the PSF. The discrete and finite sampling of visibilities leads to undesirable sidelobe patterns in the synthesized beam which makes astronomical interpretation and analysis of the dirty images difficult. The sidelobes from the brighter sources may have enough strength to obscure fainter features present in the image. In order to recover the brightness distribution of the sky we need to deconvolve the dirty image. The deconvolved image is a better estimate of the true brightness distribution. The deconvolution process minimizes the dirty and unsatisfactory appearance of the image due to sidelobe patterns and creates estimates of the visibility function at some positions in the Fourier plane where it has not been measured. In practice the dirty image is also affected by the presence of noise in the visibilities and can be written as,

$$I^D(l,m) = I^t(l,m) * P(l,m,n) + I^N * P(l,m,n) \tag{6.2}$$

where I^N is the inverse Fourier transform of the visibility noise. So any deconvolution algorithm also attempts to separate $I^t(l,m) * P(l,m,n)$ from $I^N * P(l,m,n)$. There have been several deconvolution techniques which have been developed and are used in astronomy like CLEAN (Högbom, 1974), MEM (Maximum Entropy Method) (Narayan & Nityananda , 1995), NNLS (Non Linear Least Squares) (Briggs, 1995), MM (Maximum Emptyness) (Marsh & Richardson, 1987), GSP (Gerchberg Saxon Papoulis) (Gerchberg & Saxton,

1972; Papoulis, 1975), Richardson Lucy (Richardson, 1972; Lucy, 1974) and SVD (Singular Value Decomposition) (Andrews & Hunt, 1977). All these deconvolution algorithms are nonlinear and accumulate some model of the sky which is convolved with the PSF and differenced with the dirty image yielding the residual. The sky model may posses non zero spatial frequencies out to the maximum gridded spatial frequency determined by the pixel spacing in the sky, or the spectral power may be rolled off at higher spatial frequencies due to smoothness constrains imposed by the particular algorithm (Briggs, 1995).

Algorithms like CLEAN, MEM and its variants are all scale less algorithms. The scale sensitive algorithms are also used, notably the Multi Resolution Clean (Walker & Schwarz, 1988) and Wavelet deconvolution (Stark et. al., 1994; Stark & Murtagh, 1994a, 2002). Recently Bhatnagar & Cornwell (2004) have proposed scale sensitive deconvolution of interferometric images based on adaptive scale pixel decomposition. Their work is based on the argument that in general spatial correlation length (a measure of scale of emission) is a stronger separator of signal from the noise, compared to the strength of the signal alone. Before discussing the deconvolution work carried out in this dissertation we first briefly review the earlier work carried out for deconvolving images made using the MRT.

6.2 Review of earlier work on deconvolution at MRT

The earlier work related to deconvolution has been carried out by Golap & Udaya Shankar (2001) for images with partial resolution. A CLEANed image with a resolution of $17' \times 23' \sec(\delta + 20.^{\circ}14)$ covering the RA range of 18hrs to 24hrs and 00hrs to 05hrs and the entire declination range of MRT has been made by Golap (1998). The images were synthesized using the observations from allocations 1 to 12 (block-1 and block-2) and only eight groups (first four East and first four West groups) in the center of the EW arm were used (so as to have comparable resolution in both directions). The PSF was extracted from the dirty images itself and shifted to another declination using indigenously developed Dec-shift algorithm (Golap & Udaya Shankar, 2001). The wide field images were deconvolved using the task APCLN in AIPS. Since APCLN allows usage of a single PSF, it is not very suitable to CLEAN wide field images in which the PSF is a function of position in the image. So, the entire image was divided into five zones along declination. The zone width was chosen as a function of the rate at which the beam changes its shape. Thus the zone was largest at zenith (0.25 in $\sin(za)$ domain) and was smaller for zones away from the zenith. The images in each zone were CLEANed by a single PSF appropriate to the center of the zone. Due to this the full potential of the Dec-shift algorithm could not be utilized.

The applicability of Dec-shift algorithm incase of full resolution dirty images is severely

limited. In case of the partial resolution survey only those observations which were uninterrupted for one complete day were used to obtain the entire image (for the region covered by the survey). Hence, any PSF extracted from the image could be transformed to another declination using the Dec-shift algorithm. In case of full resolution images, each sidereal hour has been imaged with different days of data (depending upon its availability). For each one sidereal hour range, the images have been synthesized separately for each of the four delay zones. Thus the PSF extraction has to be carried out for each sidereal hour and delay zone separately. In addition, extracting PSF from the dirty image is made difficult due to presence of other sources in the field apart from the point source of interest. Such sources (especially if they lie along the same RA or declination) may not be easily distinguishable from the sidelobes and we may generate an unsatisfactory PSF. Thus we would need strong sources away from the confusing regions in each delay zone for all the sidereal hour ranges covered. This situation does not exist. In addition and more importantly in the partial resolution survey, the bandwidth decorrelation effects do not play a significant role and hence ignored when transferring a PSF from one declination to another. This is not true in case of the full resolution images (See Sec. 6.3.2.2). Due to these reasons the Dec-shift algorithm has not been employed to estimate the PSF from the full resolution images presented in this dissertation.

Convolution along RA and declination :

As a simpler alternative to deconvolution, a few techniques are sometimes used to reduce the sidelobe response of the PSF in the dirty image. One of them is to convolve the image in both the directions with a correcting beam (Dwarakanath, Deshpande, & Udaya Shankar, 1990). The correcting beam can be estimated with the help of useful family of gradings whose transforms can be exactly calculated (Christiansen & Högbom, 1985). Once a correcting beam is known for both RA and $\sin(za)$, two 1-D convolutions of the dirty image can be carried out to reduce the sidelobes down to 3-4%. The disadvantage of such a convolution is that it leads to a loss in resolution by a factor of $\sqrt{2}$, in both the directions. However MRT being a non-coplanar $\top$ array, the 2-D PSF cannot be obtained by taking the product of two 1-D PSFs along RA and $\sin(za)$. Due to this, the convolution scheme is not applicable for dirty images made using the MRT. We mention below a few difficulties involved in the application of such a technique to MRT.

First, let us consider the convolution along RA. We consider a source at declination δ_1. Its sidelobe at some other declination δ_2 will have width along RA proportional to $\sec(\delta_1)$. So in order to reduce the sidelobe at declination δ_2, we need to use the correcting beam corresponding to declination δ_1. Now for a source at declination δ_2 this would be inappropriate as its beam along RA is proportional to $\sec(\delta_2)$. Thus it is not possible to meet

both these requirements with this approach. The problem in convolution along $\sin(za)$ axis is still more tricky. Let us consider a source at (RA_1, δ_1). The sidelobe of this source at (RA_1, δ_2) would have been given a height correction appropriate for a source at declination δ_2, although it is sidelobe of a source which is at declination δ_1. Due to this reason, the sidelobes peak at slightly different RA than the true RA of the source. So the 1-D PSF along $\sin(za)$ is not a *sinc* and depends upon the declination of a source. It would not be simple to come up with a correcting beam which appropriately takes care of this declination dependence of the PSF due to non-coplanarity. In addition to the above difficulties the PSF is also declination dependent due to bandwidth decorrelation. Thus even if the loss in resolution is accepted this scheme is not applicable to suppress the sidelobes of the wide field images. In view of this a deconvolution scheme was developed for the full resolution images made using the MRT which is discussed in the next section.

6.3 A deconvolution scheme for MRT

Due to the declination dependence of the PSF and images covering wide-field, we needed to come up with an appropriate deconvolution scheme. The scheme developed by us for deconvolution is based on the concept of using a minimum number of appropriate sized pre-generated look-up PSFs during deconvolution using the conventional CLEAN algorithm, for a given dynamic range. This scheme does not requires PSF interpolation in the image plane during every iteration in the CLEAN loop. We first briefly describe the CLEAN algorithm followed by a detailed discussion on the variation of the MRT PSF. Next we discuss important aspects in estimation of the PSF :- its size, the number of PSFs required and optimization of its run time performance. Later we describe the important aspects of the deconvolution procedure as applied to MRT images and present the results in form of deconvolved images.

6.3.1 CLEAN

The most popular algorithms for deconvolution which are used in radio astronomy are CLEAN and MEM. Algorithms like MEM can give a resolution better than given by the dirty beam. In the present work, our main interest is to suppress the sidelobes while retaining the resolution of the dirty beam in view of which the conventional CLEAN algorithm was used for deconvolution in this dissertation.

The CLEAN algorithm was devised by J. Högbom (Högbom, 1974) and represents the sky by a number of point sources in an otherwise empty background. The algorithm proceeds iteratively and finds the peak in the residual image at each iteration (at the start the

original dirty image and the residual image are same) at the point of highest correlation between the PSF and the residual image[1]. At the position of the peak in the residual image, a fraction of the peak, also known as loop gain (γ), is accepted as a CLEAN component. The normalized dirty beam (unit height), scaled by multiplying the product of the peak with the loop gain, after shifting to the location of the peak in the dirty image, is subtracted from the residual image. In this manner the flux is incrementally transferred from the residual image to CLEAN components. The process is iterated till the peak in the residual image reaches a desired threshold. In addition a priori information is generally used to support the CLEAN by specifying regions suspected to be due to real emission called as CLEAN windows, where the algorithm would search for peaks. The CLEAN components are convolved by a restoring beam and added to the final residual image to form a deconvolved or a restored image.

Beyond the simple Högbom algorithm, there are two major variants, the Clark clean (Clark, 1980) and Cotton-Schwab clean (Schwab, 1984) which perform essentially the same task but do so in a more efficient way. The Clark clean has the concept of major and minor cycles and uses the insight that the repeated shift, scale and add cycle of the Högbom algorithm may be done faster with the use of FFTs. As the goal of Clark CLEAN is to duplicate the Högbom CLEAN, at the cost of an additional approximation and since the computational resources to compute the original Högbom CLEAN existed, it was not considered. It is to be noted that the Clark clean is more resistant to the accumulated rounding errors than Högbom algorithm but this does not play a role in our deconvolution since the number of iterations is always less than 10^5 and thus the rounding errors are negligible. The second variant Cotton-Schwab algorithm, which also has concept of major and minor cycles like Clark clean with the difference that during a major cycle the model components are subtracted not form the original dirty image but from the original visibility data (uv clean). The major advantage is that aliasing due to convolutional griding is significantly reduced and multiple fields can be deconvolved simultaneously. Since the images in this dissertation consist of single fields which are sufficient to cover all the emission, the cotton Schwab algorithm was also not considered.

The central key aspect of Högbom CLEAN used in our scheme is the knowledge of dirty beam or the PSF. In view of this we now discuss the PSF of MRT and its variation in the next section.

[1]This is only strictly true for the uniformly weighted PSF, but in practice is approximately so for all the PSFs encountered in radio interferometry (Briggs, 1995).

6.3.2 The Point Spread Function (PSF)

The PSF is the response of the array to a celestial point source in the sky. It determines two important characteristic features of the dirty image : the resolution and the dynamic range. The $\top$ array is used in a correlation mode in which the EW array is multiplied with the NS array. Thus the observed PSF is the 2-D PSF of EW array multiplied with the 2-D PSF of NS array. The PSF and the aperture illumination form Fourier pair and the PSF can be generated from the aperture illumination. We use the real beam and the corresponding real image for deconvolution. The true PSF of an array can be generated from the gain and phase of every baseline used in the array. The resulting PSF $P(l,m,n)$, is the weighted sum of *cosines* corresponding to the measured Fourier components.

$$P(l,m,n) = A(l)\frac{\sum_{\forall k} W_k(u_k,v_k,w_k)\, f_k(m) cos(u_k l + v_k m + w_k n)}{\sum W_k\, f_k(m)} \tag{6.3}$$

where k refers to different baselines, $A(l)$ is the normalized primary beam response of the interferometer formed by the EW and the NS groups [2], $W_k(u_k,v_k,w_k)$ is the weighting sampling function which is non zero only for the sampled points in the uv plane and $f_k(m)$ is the factor due to the bandwidth decorrelation. The PSF is a collection of *cosines* and extends forever in the image plane. The sidelobes drop off as the inverse of distance from the source location in the image plane along the RA and declination directions. The HPBW is of the order of $\frac{1}{u_{max}}$ and $\frac{1}{v_{max}}$ where u_{max} and v_{max} are the maximum lengths of the baseline measured.

The PSF of an array generally changes with direction due to different uv coverage when viewed from different directions. For small fields, the change is small and may be neglected but for a wide field the variation can be significant and has to be taken into account. In case of MRT, due to meridian transit imaging the change would be due to different projections of the NS baselines when viewed from different declinations. Since our images are in $\sin(za)$ coordinate system, the 1-D scan of the beam along the declination on the meridian remains invariant due to this effect. However, there are various other factors on which the PSF of the MRT depends such as non-coplanarity of the array, bandwidth decorrelation, precession, variation of beam in RA with declination and interference. These are discussed in the following sections.

6.3.2.1 Non-coplanarity of the array

As discussed in Chapter 5, the Fourier inversion of the visibilities measured by a non-coplanar array gives the three dimensional image volume function $F(l,m,n)$ (Perley, 1999),

[2] This term arises due to meridian transit imaging. The primary beam response along l direction (hour angle) has to be taken into account while computing the PSF.

$$F(l,m,n) = \frac{\left[I(l,m)\delta(\sqrt{1-l^2-m^2}-n)\right]}{\sqrt{1-l^2-m^2}}$$

where, the image volume is a function of three variables but meaningful quantities within it lie on a sphere of a unit radius defined by $n = \sqrt{1-l^2-m^2}$. Since in practice we know only the sampled coherence function $S(u,v,w)V(u,v,w)$ where $S(u,v,w)$ is the sampling function describing the location of the samples of the visibility. It is zero at all positions except where the visibilities have been measured. The convolution theorem can be used to show that the result of Fourier inversion becomes,

$$F(l,m,n) = \frac{I(l,m)\delta(\sqrt{1-l^2-m^2}-n)}{\sqrt{1-l^2-m^2}} * P(l,m,n) \tag{6.4}$$

which can be simplified to,

$$F(l,m) = \int I(l_o,m_o)P(l-l_o, m-m_o, \sqrt{1-l^2-m^2} - \sqrt{1-l_o^2-m_o^2})\frac{dl_o dm_o}{\sqrt{1-l^2-m^2}} \tag{6.5}$$

Now let us consider an isolated point source in the sky. As the point source drifts in the sky transiting the meridian, its direction cosines l', m' change with the Hour Angle (HA). The dirty image when the point source is at (l', m') is given by,

$$\begin{aligned} F_{PSF}^{(l',m')}(l,m) &= k\int \delta(l_o-l', m_o-m')P(l-l_o, m-m_o, \sqrt{1-l^2-m^2} - \sqrt{1-l_o^2-m_o^2})dl_o dm_o \\ &= kP(l-l', m-m', \sqrt{1-l^2-m^2} - \sqrt{1-l'^2-m'^2}) \end{aligned} \tag{6.6}$$

where k is a constant. At the meridian l=0, m=$-sin(za)$. Then the PSF, $F(0,m)$ for various values of l' is given by,

$$F_{PSF}^{(l',m')}(0,m) = kP(-l', sin(za') - sin(za), cos(za) - cos(za'))$$

The above function, functionally depends on the term $\sqrt{1-l^2-m^2} - \sqrt{1-l'^2-m'^2}$, which is introduced due to non-coplanarity (Golap & Udaya Shankar, 2001). This extra dependence is simply the difference of the distance from the origin of the point at which we want to estimate the function (*i.e* (l,m)) and the distance of the center of the point source from the origin. Thus the PSF will have different shapes depending on where the point source is centered. This implies that for deconvolution of the antenna response from the 2-D image, we need different functions which depend upon the zenith angle of the source being deconvolved.

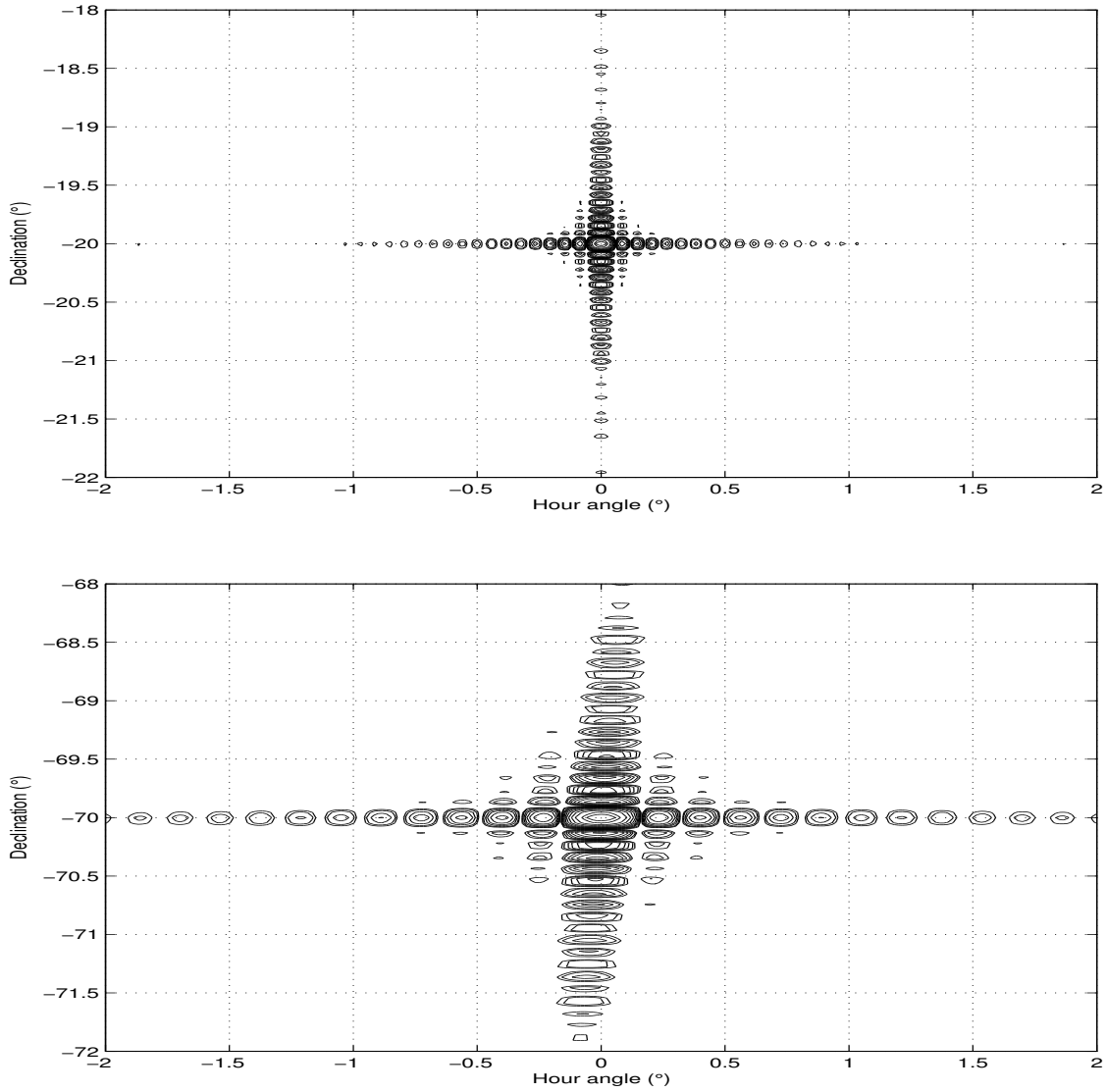

Fig. 6.1: Contour representation of the declination dependent PSF of MRT. The upper plot shows the PSF for a source at declination of -20° while the lower plot shows the PSF for a source at a declination of -70°. The sidelobe along declination peak at different RAs rather than the true RA of the source due to non-coplanarity (the effect can be seen more pronounced in the lower plot). We also notice the natural stretching of the FWHM of the beam in RA as sec(δ).

During the meridian transit imaging, we correct for phases at each point along the declination on the meridian. This ensures that all sources on the meridian get correctly phased and peak on the meridian. On the other hand, their sidelobes at any declination on the meridian, are phased for declination where they appear and not for source position. This causes dephasing due to which the sidelobes get attenuated. However, the extra height phases from the EW group add more or less to zero, when the point source is at some other hour angle. Thus, the sidelobes peak at an RA which is different from the RA of

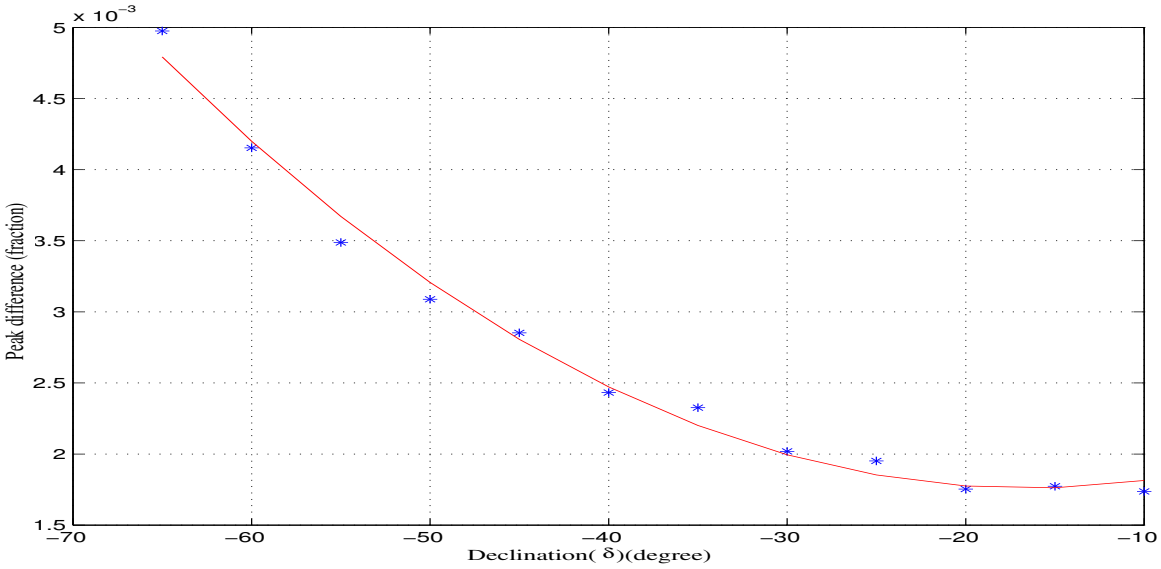

Fig. 6.2: This plot shows the peak difference (as fraction) between the PSF at the tangent point and a PSF at the end of a 5° zone for various zenith angles of the tangent point (Oozeer & Udaya Shankar, 2002). The maximum difference is ≈0.5%. The solid line shown is a second order polynomial fit.

the point source. Now the position and the strength of the sidelobe depends upon how far it is from the field center, the zenith angle of the source, and the EW height distribution. This results in a twisted PSF as shown in Fig. 6.1.

To get a quantitative estimation of the height effect due to non-coplanarity, a simulation study was carried out by Oozeer & Udaya Shankar (2002). They divided the sky into zones of ±5° in declination and calculated the peak difference[3] between the PSFs generated at the tangent point (centre of the zone) and at the edge of the zone[4]. This gave an estimate of the dynamic range if only one PSF at the center of the zone is used to deconvolve an image covering ±5°in declination. Their estimation was carried out assuming uniform illumination of the aperture. Fig. 6.2 shows the maximum difference between the PSF at the tangent point and a PSF at the end of a 5° zone as a function of the declination of the tangent point.

Their analysis revealed that the maximum error is ≈0.5% when the PSF at zenith angle, za=-45° was used for the zone corresponding to the zenith angle range -50°to -40°. The maximum error was less for other zones. For the zone covering the zenith angle range from -20° to -10°, the maximum error is only 0.18%. Thus for a dynamic range limit of 200, the approximation of a PSF at any declination with a one at 5°away is permissible. If we consider the noise in the images as ≈200 mJy beam^{-1}, we will be dynamic range limited only

[3]It is to be noted that peak difference or maximum difference between two PSFs refers to the maximum absolute difference between two normalized PSFs.

[4]Since their aim was to investigate the effect of non-coplanarity on the PSF, they carried out simulations in l, m domain. The effects of bandwidth decorrelation was ignored during the simulations.

for sources which are stronger than 40 Jy. In the southern sky covered by the declination range of MRT if we use the MRC (Large et. al., 1981) catalogue at 408 MHz and assume a spectral index of 0.7 between 408 and 151.5 MHz, there are only 23 such sources, which are expected to be stronger than 40 Jy at MRT. Thus using 6 PSFs across the entire declination range of MRT for a dynamic range of 200 is a good target.

6.3.2.2 Bandwidth decorrelation

Although we use uniform weighting as discussed earlier (Sec. 5.4.4), a factor which modifies the effective weighting and hence the PSF, is the bandwidth decorrelation. Modern telescopes use FX correlators in which the observing band is divided into a large number of narrow frequency channels and the effect of bandwidth decorrelation is generally insignificant. At MRT we use an XF correlator. Due to meridian transit imaging there is no decorrelation along RA. We measure the visibilities with a 1 MHz bandwidth with four different delay settings where with each delay setting, a part of the declination range (known as a delay zone) can be imaged without appreciable decorrelation ($< 20\%$) (See Table 5.3; Sec. 5.4.3). However, each delay zone still covers a wide field of the sky ($\approx 15^\circ$-20° in declination) and the effect of bandwidth decorrelation on the PSF needs to be estimated.

In general, the bandwidth decorrelation depends upon the baseline along the NS. We can approximate the delay curve, as a function of baseline to be a step function, where each step corresponds to 84 m in the NS (one allocation). The bandwidth decorrelation manifests itself by changing the effective weighting during the co-addition of each day images and hence the PSF. In our present scheme the relative weights in each day's image are estimated using the amplitude gain by fitting a well known strong point source. In the first stage, when the images of the same allocation (and hence the same baseline configuration) are combined, the bandwidth decorrelation at any declination being same, there is no change in the PSF. In the next stage when the resultant images of different allocations are co-added using the relative weights determined by fitting for a well known strong point source, the effective weight at any declination δ_p for an allocation's image is modified by the ratio of correlation response at δ_p and the correlation response at the source declination δ_s, which has been used to determine the relative gains. This can also be expressed as,

$$f_d(\delta_p) = \frac{C_d(\delta_p)}{C_d(\delta_s)} \tag{6.7}$$

where $f_d(\delta_p)$ is the factor by which the effective weighting for each day's image gets modified due to bandwidth decorrelation at the declination δ_p. $C_d(\delta_p)$ is the correlation

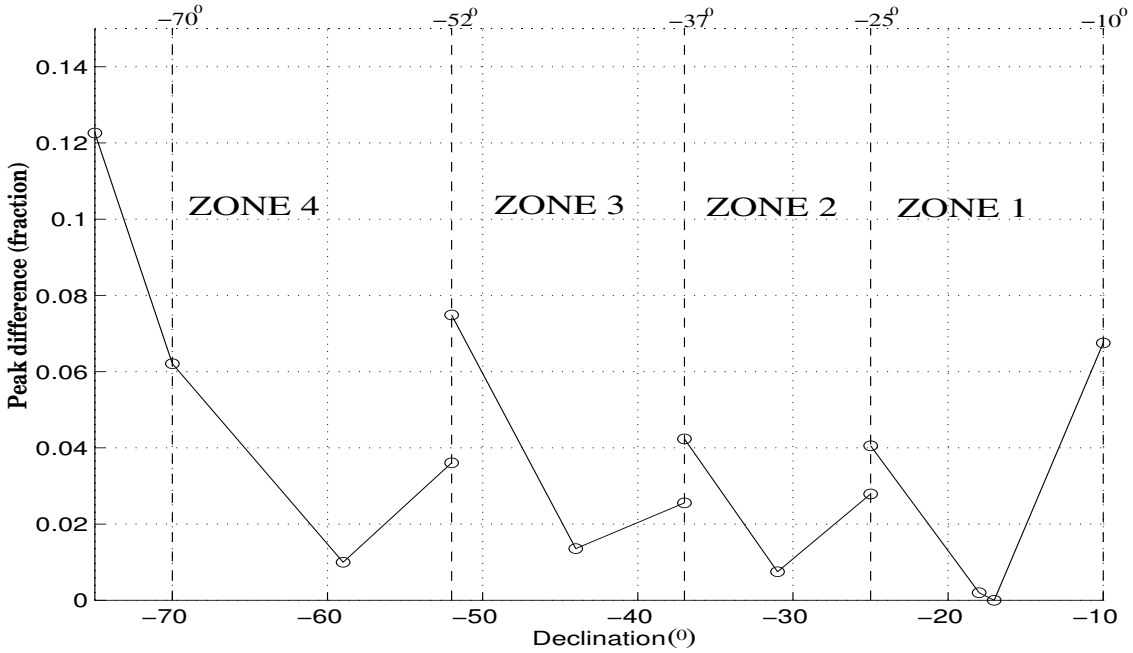

Fig. 6.3: The plot shows the peak difference (as fraction) between PSFs estimated at the same declination with and without including the effects of bandwidth decorrelation. The maximum difference in PSFs can be as much as 12.5% at δ=-75°. We also note that in the regions of overlap between two delay zones the effect of bandwidth decorrelation on the PSFs in the two zones is different. For example at δ=-52°, the error due to neglecting bandwidth decorrelation in zone 3 is 7.5% while in zone 4 it is only 3.75%.

response at the declination δ_p (in the delay zone for which the PSF needs to be estimated) and $C_d(\delta_s)$ is the correlation response at the declination δ_s (in the delay zone of the source used to estimate the relative gains on different days).

A quantitative study was carried out to estimate the effect of bandwidth decorrelation on the PSF. The simulations were carried out in (RA,sin(za)) domain. PSFs were estimated with and without taking into account the effect of bandwidth decorrelation. Fig. 6.3 shows the maximum difference between the PSFs calculated with and without including the effect of bandwidth decorrelation for sources at various declinations in the four delay zones. The source used for estimating the amplitude gains in each day's image was MRC2211-172 (lies in the first delay zone). From the plot we note that the maximum error in a PSF calculated without considering the effect of bandwidth decorrelation in the entire declination range (-10°to -70°) is ≈7.5%. The error further increases rapidly for sources outside this declination range and increases up to ≈12.5% at δ=-75°. Hence, the effect of bandwidth decorrelation cannot be neglected during estimation of the PSF. We also note that for the regions of overlap between two delay zones, the errors in neglecting the bandwidth decorrelation in the estimation of the PSFs are different. For example at δ=-52°, which lies

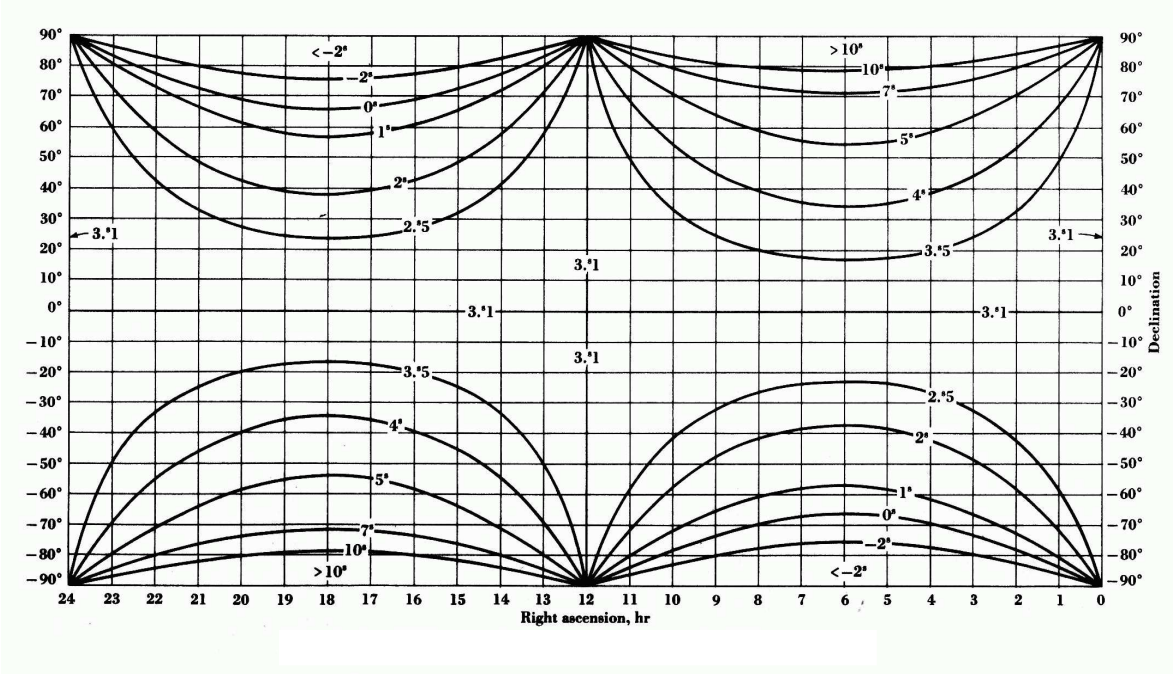

Fig. 6.4: Right-ascension precession in seconds of time per year (figure taken from Kraus (1988a)).

in both the delay zones 3 and 4, the maximum error in the PSF ignoring the bandwidth decorrelation is 7.5% and 3.75% respectively. When the source used to estimate the relative gains lies near the extreme ends of the delay zone boundary, the maximum error due to neglecting the bandwidth decorrelation are higher.

6.3.2.3 Precession

As described earlier each allocation's image is box-car averaged for four integration periods (≈4 s) and precessed from the epoch of observation to a common grid in the epoch J2000, before being co-added with appropriate weights to obtain the full resolution image (Sec. 5.4.1). Since the precession depends on the RA and declination, this causes the sidelobes to be precessed differently than the source main beam. Hence, the deconvolution of such an image would require a PSF which is a function of both RA and declination. Such an image would be practically very difficult to deconvolve owing to the computational and memory resources needed. We have used observations carried out over a span of ≈ 5 years. The differential precession between the source and the sidelobes would depend upon the region of the sky under consideration and the day's on which data for different allocations was used to obtain the full resolution image. Fig. 6.4 shows the precession per year for different RA and declination. We note that the differential precession between declination δ=0° and δ=-70° at RA 18 hrs can be up to 4 s per year. The error in the PSF due to differential precession of the sidelobes and the main beam depends upon two competing factors. The differential precession between the source and its sidelobes

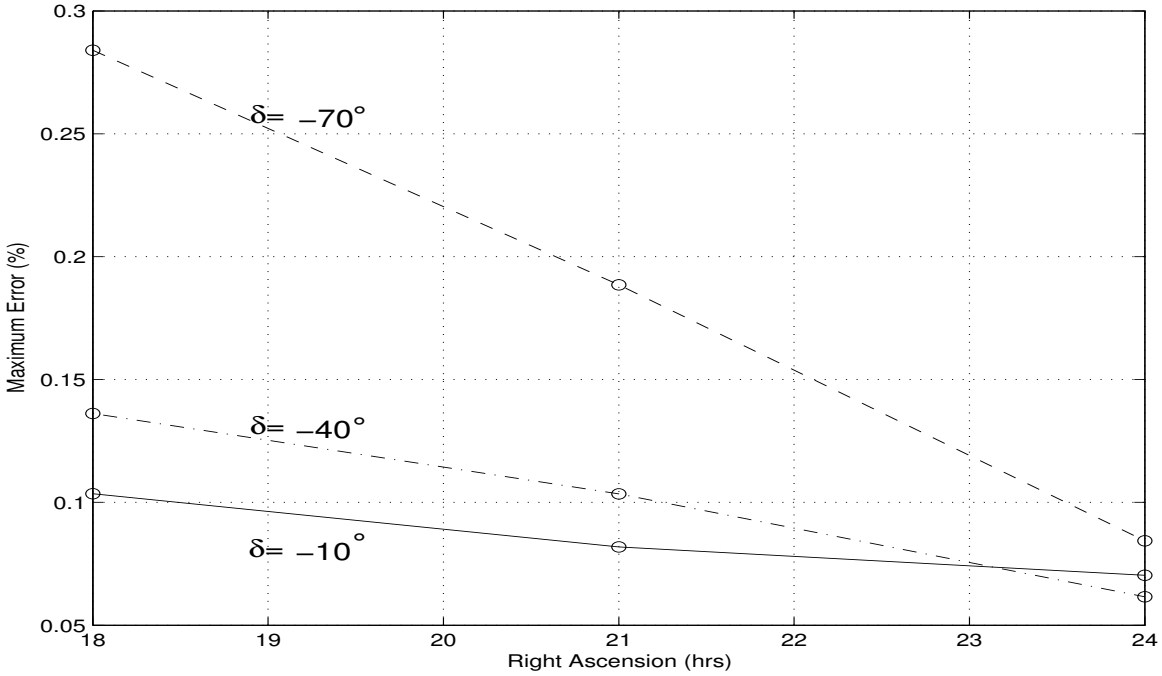

Fig. 6.5: The maximum error in the PSF of a source at different positions in RA and declination due the differential precession of the sidelobes. The maximum error is ≈0.28% (for a source at RA of 18 hrs, δ=-10°). The error is generally higher for lower declinations (away from the equator). The positions where the maximum error was actually estimated is shown by open circles.

increases with the increase in distance of the sidelobe from the source, but at the same time the amplitude of the sidelobes farther away itself gets progressively reduced.

In order to estimate the change in the PSF due to differential precession, a quantitative study was carried out. In the simulations we used the mean epoch as January 1, 1997 and studied the effect of precession on the PSF to J2000 epoch. We considered sources at RA 18:00 hrs, 21:00 hrs, 24:00 hrs and for each hour at three declinations -10°, -40°, -70°. Fig. 6.5 shows the result of the simulation. The simulations indicate that the maximum error by ignoring the effect of this differential precession between the source and its sidelobes in the dirty images is ≈0.28%. The maximum error depends on declination and it decreases for declinations closer to the equator. Thus the change in the PSF due to differential precession is not significant for the dynamic range aimed and hence can be neglected in the estimation of the PSF.

6.3.2.4 The variation of PSF in RA

If the effects of bandwidth decorrelation and the non-coplanarity are ignored, the PSF is invariant in l, m domain. However, due to the ease of choosing the (RA,sin(za)) coordinate system in the meridian transit mode, the FWHM of the beam along RA varies with declina-

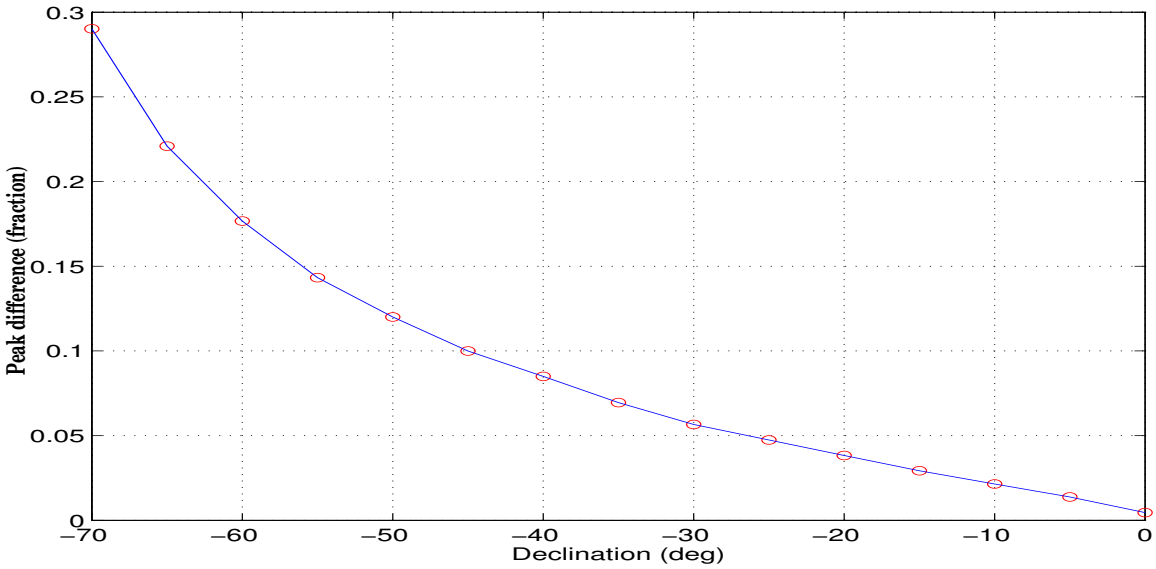

Fig. 6.6: The peak difference (fraction) between the PSFs generated for a source at a declination δ and for a source at declination (δ-5°), as a function of declination (δ), due to the variation of beam in RA as $sec(\delta)$. The maximum error is ≈28% at δ=-70°.

tion ($beamwidth \propto sec(\delta)$). The rate of change of the beam in RA increases as we go towards declinations away from the equator. This aspect has to be taken into account while estimating the PSF for deconvolution. However, since at the meridian m=-sin(za), the beam is invariant along sin(za).

A quantitative estimate of the error for this variation of beam in RA with declination was carried out. Fig. 6.6 shows the maximum difference between the PSFs at two different declinations separated by 5° (The non-coplanarity and the bandwidth decorrelation were not taken into account in estimation the PSFs). From the plot we note that the error can be as high as 22% if a PSF at δ=-65° is approximated by a PSF 5° away at δ=-70°. This error is unacceptable. Thus the deconvolution procedure needs to take into account the variation of beam in RA on the PSF.

6.3.2.5 Effect of interference

Interference detection is carried out in several stages of data processing (Chapter 4) but its actual excision is implemented at two stages[5]. In the first stage during post-integrating each day's image along RA for 4 seconds, we give zero weights to the visibilities affected by interference (detected up to the level of each day's image before post-integration). As-

[5]We recall that the interference is also removed in the self correlation measurements with the AGC (Sec. 4.3.4) and total power measurements without the AGC (Sec. 7.2.1.3), but it has no bearing on the PSF and thus not considered here.

suming visibility corresponding to one of the integration periods (≈1.1 s) is affected by interference during the post-integration, giving it zero weight simply results in a decrease in the signal to noise ratio of the image pixel obtained after post-integration (≈0.85 of the original). If we assume interference to be present at a given sidereal time in only one allocation's image, then in the final images obtained after co-adding images of 63 allocations the net effect on the signal to noise ratio at the affected RA would be negligible (≈0.0012%). Hence the effect of this first stage of interference excision on the PSF can be neglected.

In the second stage the interference which is detected collectively using the combined data set of all the post-integrated images is excised during the co-addition of each day's image with appropriate weights, to obtain the full resolution dirty image. During the co-addition, the entire 1-D image scan along the declination at the sidereal time affected by interference in each day's image, is obtained by linearly interpolating the adjacent 1-D scans which are not affected by interference. If the effect of interference is significant on the PSF, it would result in a PSF which is also a function of location of interference relative to the source position. Hence, deconvolution would become intriguingly complicated. Since the interference points are scattered and very few in each day's image (allocation), we expect the error made in the PSF estimation without taking interference excision into account to be negligible.

Estimation of the effect of interference on the PSF is not straightforward as it depends upon the distribution of interference on each day and the number of days the interference is present at the same sidereal time. However, if we assume that at a given sidereal time, data of only one day's images is affected by interference, we can estimate the error in the final image formed by combining all the 63 one day images. The magnitude of this error will depend upon the allocation affected by interference and the hour angle at which the interference occurs from the source position. Since interference can be in general at any arbitrary sidereal time and in any allocation's image, we varied the position of interference in each allocation's image as a function of hour angle. Fig. 6.7(a) shows the maximum fractional error as a function of hour angle of the interference position from the source and the allocation number effected by interference. From the plot we note that the error is maximum when the interference occurs at the source transit in an allocation's image. However, the magnitude of this maximum error is only ≈0.13% which can be ignored. In fact even if there is interference at the same sidereal time in the images of three allocations (which is less likely to happen as shown by the interference statistics), the errors would still be negligible. It is to be noted that this error due to neglecting the interference excision in the PSF is maximum for a source transiting at the sidereal time at which interference occurs. The error drops rapidly (since the beam along RA is 16 s wide the interpolation also has a

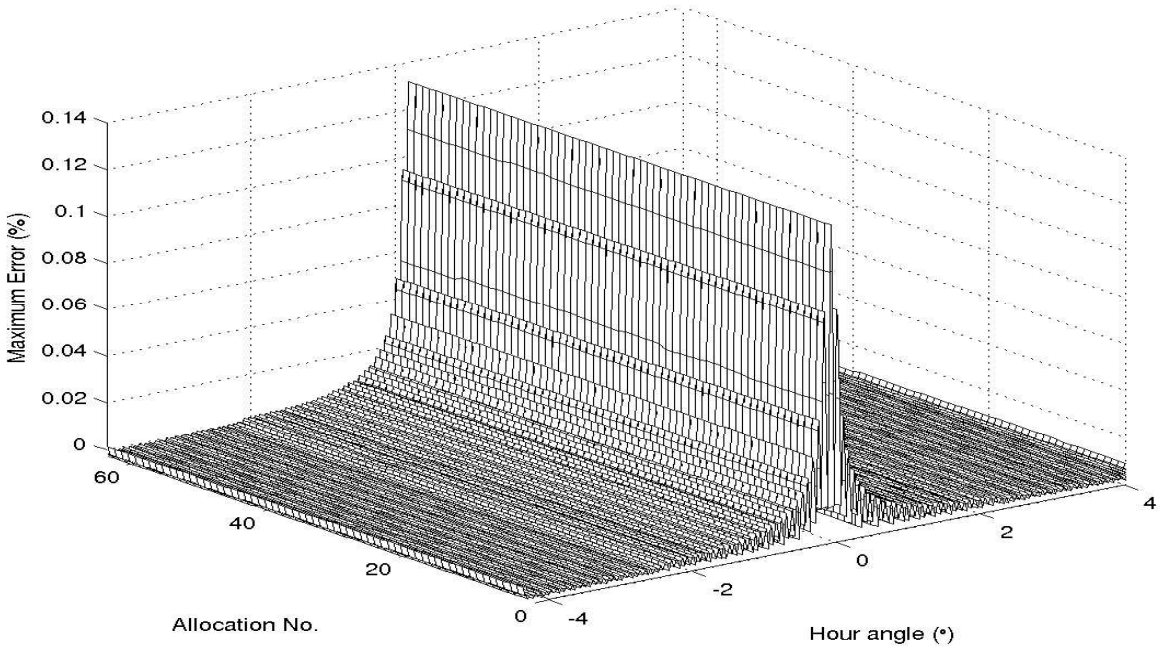

(a) Error in PSF when interference in one day's image is flagged and the intensity on the 1-D image scan at the affected RA is estimated by linearly interpolating the 1-D image scans at the adjacent RAs unaffected by interference (in the image in which it occurs). The maximum error is 0.13%.

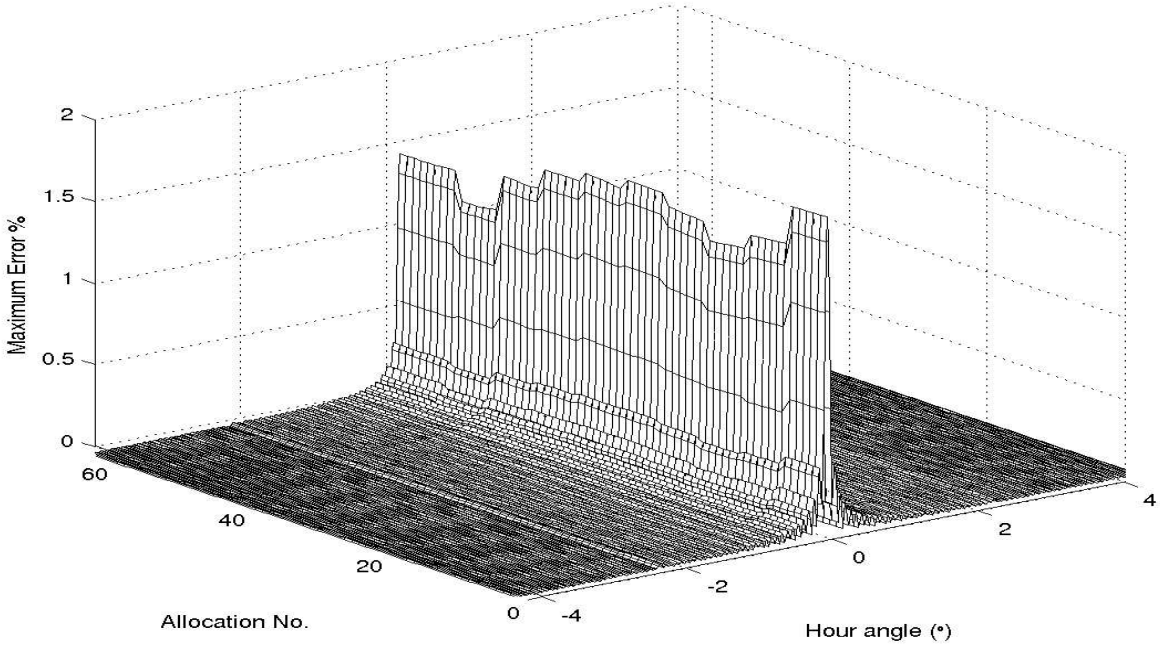

(b) Error in PSF when interference in one day's image is flagged and the 1-D image scan at the affected RA (in the image in which it occurs) is given zero weight while co-adding the images. The maximum error is 1.95%.

Fig. 6.7: Error in full resolution PSF (using 63 allocations) when interference occurs in any one allocation's image at a given sidereal time. The y-axis shows the allocation number of the image in which the interference occurs and the x-axis shows the hour angle of interference position from the source for which the PSF is estimated. The z-axis shows the maximum fractional error.

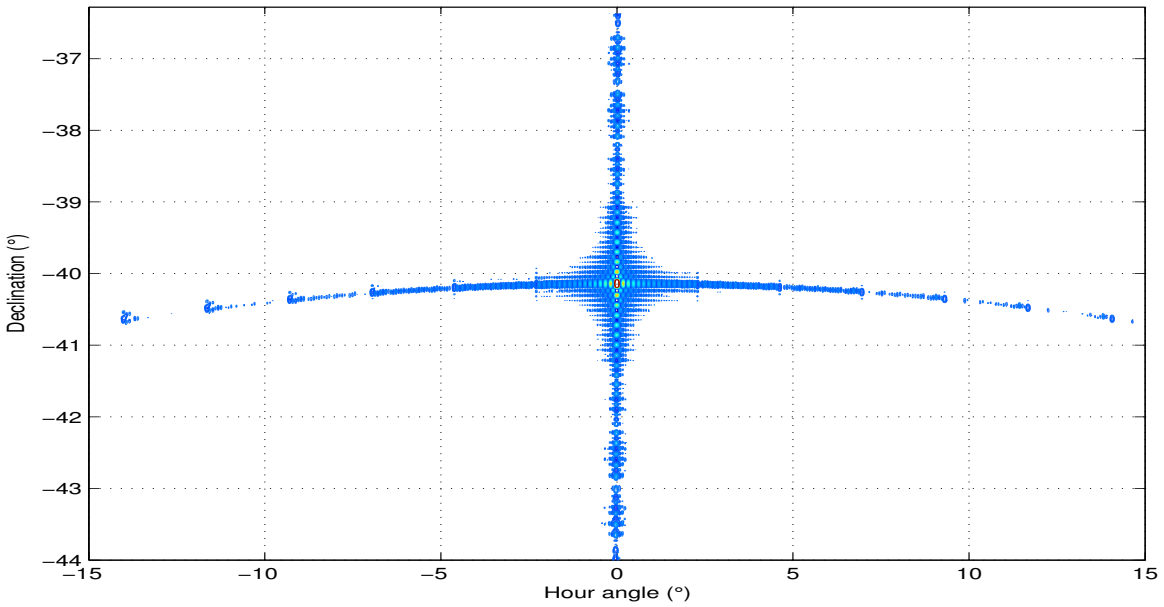

Fig. 6.8: The plot shows the curvature of the sidelobes in RA as a function of Hour Angle (HA) of a source from the meridian due to meridian transit imaging.

similar effect) with increasing hour angle from the source position. Thus the errors due to interference on the PSF can be neglected.

It is interesting to see the case if during the co-addition of individual allocation images affected 1-D image scans along declination would have been given zero weights instead. Fig. 6.7(b) shows the maximum fractional error as a function of hour angle of the interference position from the source and the allocation number affected by interference. The maximum error in the PSF still occurs when the interference is at the sidereal time of the source transit (HA=0°) but its value can increase up to 1.95% (a factor of 15 higher than the earlier case). This would have limited the dynamic range of deconvolution using such a PSF to ≈ 50. In addition, if there is interference at the source transit in more than one day's image, the dynamic range limitation would have been further limited.

Curvature of sidelobes in RA :

An interesting aspect of meridian transit imaging is the curvature of the RA sidelobes of the PSF (Dwarakanath & Udaya Shankar, 1990). This arises because the source goes through different NS beams of the telescope at different hour angles. For a source at transit, the response is at declination δ_s of the source. As the hour angle (HA) of the source changes the apparent zenith angle (za) of the source is given by the expression

$$za = \arccos\{-(\cos\delta\ \cos\ HA\ \sin\phi - \sin\delta\ \cos\phi)\}$$

where ϕ =-20.°14 is the instrumental latitude. Due to this, the response of the source is towards negative declinations for MRT resulting in the curvature of RA sidelobes which is

shown in Fig. 6.8. It may be noted that the curvature is gradual and is noticeable only for large hour angles. This curvature is automatically taken into account during the estimation of the PSF.

6.3.3 PSF estimation

Now we discuss the practical procedure for the estimation of the PSF for the full resolution images. The PSF is estimated using the fact that it is the Fourier transform of the aperture illumination (using Eqn. 6.3). We first discuss two important issues of PSF estimation, namely the size of the PSF required and the number of PSFs needed to carry out the deconvolution for MRT. The estimation of PSF is computationally expensive and time consuming. In this context we later discuss the method developed for optimization of its run time performance.

6.3.3.1 Size of the PSF

The extent of the PSF to be used for deconvolution is decided by the basic criteria that the last sidelobe should be less than the rms noise in the image. Due to this, the extent of the PSF to be used depends upon the strength of a source and the rms noise in the map. The HPBW of synthesized beam in RA varies (in time) with declination as $16\sec(\delta)$ s. The HPBW of the beam along $\sin(za)$ is constant[6] (0.01333 in $\sin(za)$ domain).

Let us estimate the number of sidelobes in both the directions for a PSF of a given size (number of pixels). In the images and the PSF, the sampling between the pixels is 4 seconds along the RA axis while along the $\sin(za)$ axis, the sampling between the pixels is 2/4095. For a PSF of size $N_{ra}\times N_{\sin(za)}$ pixels, the number of sidelobes on each side of the peak are $\approx 0.15 N_{ra}\cos(\delta)$ in RA and $\approx 0.22 N_{\sin(za)}$ in $\sin(za)$ assuming the PSF to be a *sinc* function[7]. For a PSF of size 513×513 pixels, the number of sidelobes on each side in RA is $76\cos(\delta)$ which depends upon declination while the number of sidelobes on each side in $\sin(za)$ is ≈112. Along RA this extent corresponds to ≈74 sidelobes (dynamic range 232) at δ=-10°, while at δ=-70° it contains only ≈26 sidelobes (dynamic range 81). Along $\sin(za)$ the extent of 112 sidelobes on either side corresponds to an upper dynamic range limit of 350. Taking the expected rms noise in the images as 200 mJy beam^{-1}, only sources with flux densities exceeding 70 Jy would have their sidelobe levels along declination beyond the extent covered in the PSF, higher than the rms noise. In view of this we have fixed the size of the PSF in declination as 513 pixels. At zenith this is equivalent to an angular extent of ≈15°.

[6] if we ignore the effect of bandwidth decorrelation.

[7] The approximation of assuming the PSF as a sinc function is only to roughly calculate the number of sidelobes in a PSF of a given extent.

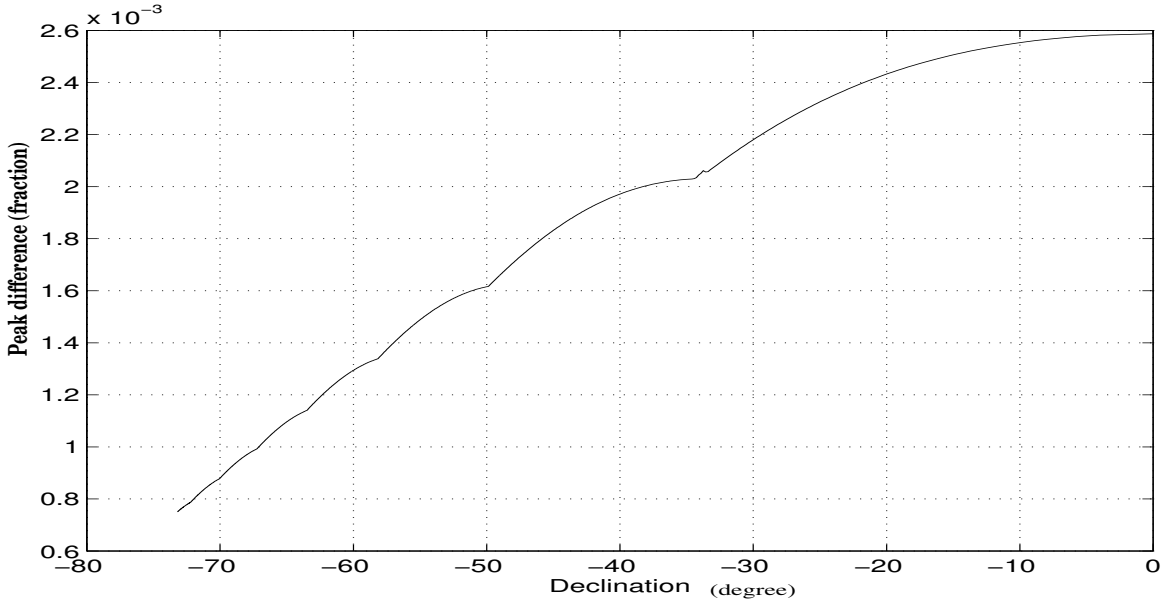

Fig. 6.9: The peak difference between two consecutive PSFs for a source at declination δ_o and at declination $\delta = sec^{-1}\{sec(\delta_o) + k\}$ as a function of δ_o. Here k is a constant given by $k = sec(4^\circ) - sec(0^\circ)$. The difference in the consecutive PSFs progressively decreases when they are at lower declinations (away from the equator).

The extent of the PSF required along RA for a given dynamic range limitation depends upon declination. For example, for an image with an rms noise of 200 mJy, any source at δ=-70° whose flux density exceeds 16 Jy would have its sidelobe along RA beyond the extent covered by the PSF (513×513) higher than the rms noise. But, for a source at δ=-10° its sidelobes along RA beyond the extent covered by the PSF (513×513), would be more than the rms noise only if its flux density exceeds 56 Jy. In view of this we adopted a two fold approach. We fixed the default size of the PSF as 513×513 (≈9°×15°at zenith) pixels. In order to take care of sources which are still bright enough to have their sidelobes beyond the extent covered in the default PSF higher than rms noise, we used a PSF of larger extent in RA of 1025×513 pixels (≈18°×15°at zenith). A source at a declination δ is considered as a bright source if the last sidelobe covered in the default PSF has an intensity higher than the rms noise. This condition can also be written as,

$$\frac{S}{\sigma} > 76\,\pi\,cos(\delta) \tag{6.8}$$

where S is the measured peak strength of the source in the image and σ is the rms noise in the image.

6.3.3.2 The number of PSFs

Once the size of the PSF is decided, the next step is to decide the number of PSFs required and how they should be distributed in declination. From the discussions in the previous section, about the various factors which affect the PSF, three effects which were found to be significant are the non-coplanarity of the array, bandwidth decorrelation and the varying beam in RA with declination as $\sec(\delta)$. For a dynamic range limitation of 200, the non-coplanarity can be handled by considering 4 PSFs in each delay zone ($\approx 35^\circ$ extent in declination). The variation due to bandwidth decorrelation can also be handled by ≈7-8 PSFs in each delay zone ($\approx 35^\circ$ extent in declination) for the same dynamic range limitation. As explained earlier the effect which causes fastest variation of the beam with declination is due to the variation of beam in RA. This can be incorporated by appropriately resampling the PSF on the fly or by interpolation using the adjacent PSFs in declination. The disadvantage in this approach is in addition to the errors which may be introduced due to interpolation, it has to be carried out for each iteration during the CLEAN. Since we use low loop gain (γ=0.05) to take care of extended features, the number of iterations required for a typical image can be as high as 15,000-25,000. This would make deconvolution computationally expensive and will slow it down significantly.

Use of look-up PSFs : In view of this we decided to use the look-up table approach by using pre-generated PSFs as and when required during the deconvolution. This approach is computationally expensive in the initial stages during estimation of the PSFs but later significantly accelerates the deconvolution process. Our aim is to generate the minimum number of PSFs at sufficiently close intervals so as the PSF for a source at any declination in the entire declination range can be approximated with the nearest available PSF without significant errors. For a dynamic range of 500 (the maximum dynamic range in principle possible using a PSF of size 513 pixels in $\sin(za)$ is 350), the maximum permissible difference between the two consecutive PSFs should be less than 0.4%.

Distribution of PSFs in declination for a given dynamic range :

In order to get a rough estimate of the number of PSFs needed and their distribution in declination we estimated PSFs at different declinations separated by equal intervals in $\sec(\delta)$ domain (as the variation in PSF is maximum due to this variation of beam in RA). Fig. 6.9 shows the maximum difference between two successive PSFs at uniform intervals of $\sec(\delta)$ as a function of declination (The maximum difference between the consecutive PSFs in declination shown in the figure corresponds to an upper dynamic range limit of ≈750). We note that the maximum difference between two consecutive PSFs reduces towards lower declinations (away from equator). Thus the sampling should be progressively

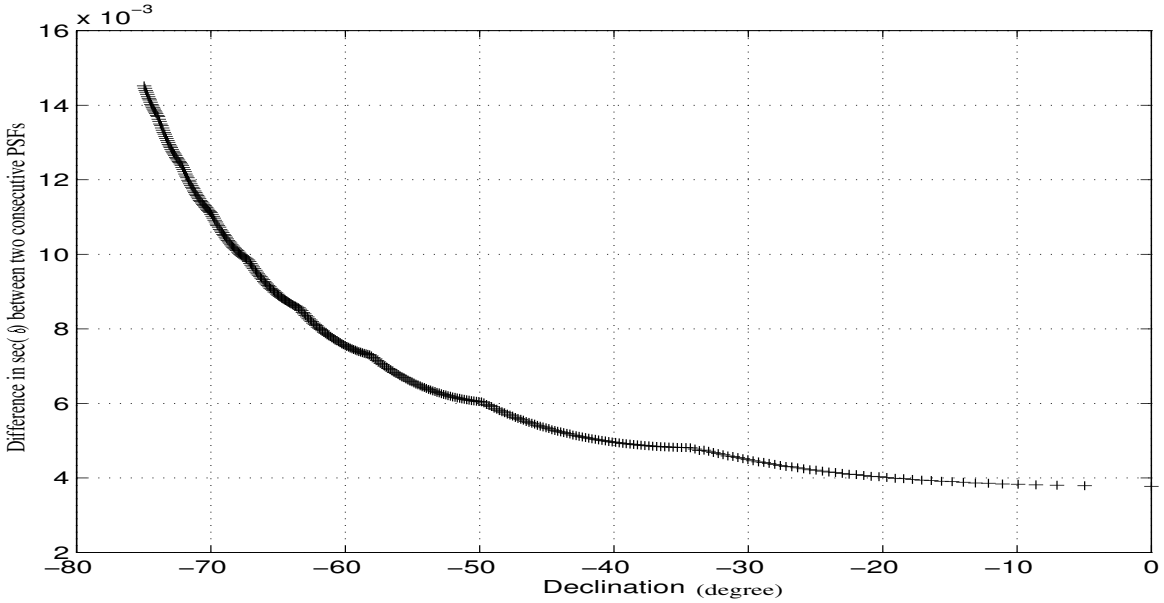

(a) The consecutive sampling required in the $\sec\delta$ domain where δ is the declination, at which the PSFs need to be estimated so as to achieve a constant maximum difference between the consecutive PSFs.

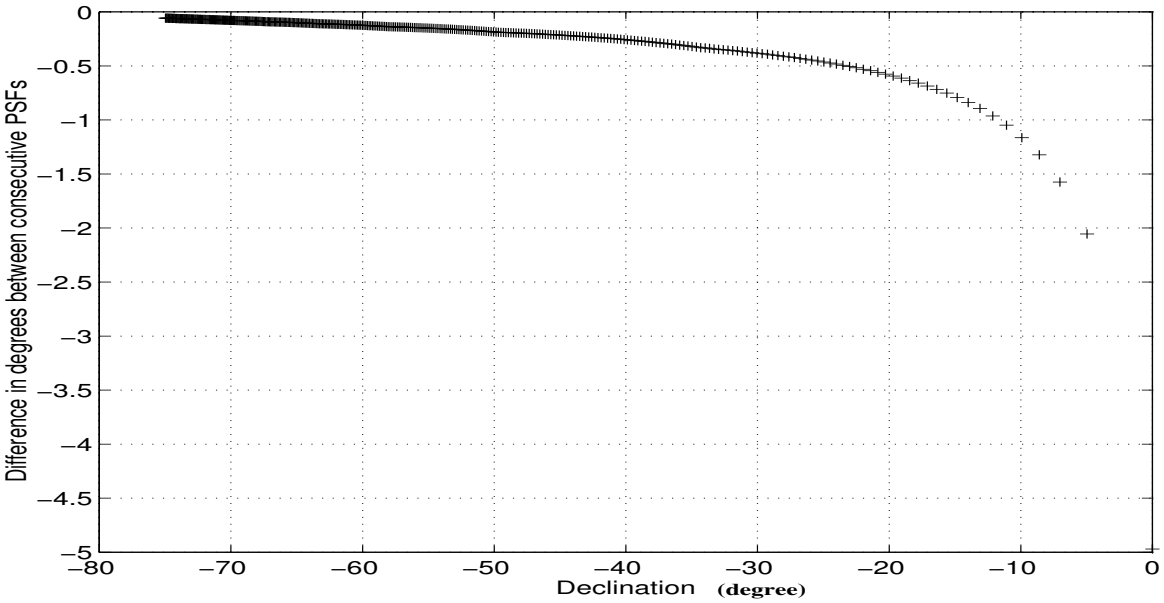

(b) The consecutive sampling required in the declination (δ) domain at which the PSFs need to be estimated so as to achieve a constant maximum difference between the consecutive PSFs.

Fig. 6.10: Sampling required in the $\sec(\delta)$ and declination (δ) domain respectively at which the PSFs need to be estimated so as to achieve a constant maximum difference between the consecutive PSFs for a dynamic range limitation of 500.

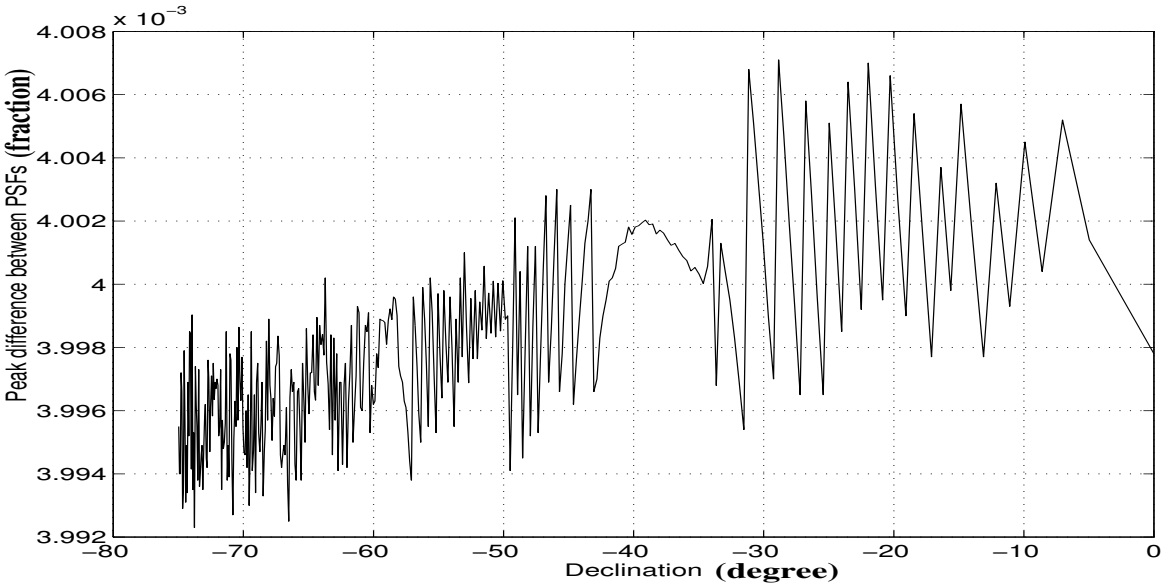

Fig. 6.11: The peak difference (as fraction) between the two consecutive PSFs which have been used to deconvolve the full resolution dirty images. The maximum difference is ≈0.4% (for a dynamic range limitation of 500). The difference is constant and varies only by a factor of 1.003 across the entire declination range.

lesser in $\sec(\delta)$ domain towards lower declinations. The relative modification required in the sampling rate would be of the order of inverse of the difference in the rate of change from one end to another.

Using this information, we estimated the required sampling between the PSFs such that the maximum difference between two successive PSFs is ≈0.4% which also gives the minimum number of PSFs needed. Fig. 6.10 shows the sampling interval in $\sec(\delta)$ and declination required between the successive PSFs as a function of declination for a limiting dynamic range of 500 without any interpolation. We note that in the $\sec(\delta)$ domain the PSFs are simulated at progressively increased intervals towards lower declinations, while in the declination the sampling becomes finer.

Fig. 6.11 shows the maximum difference between two successive PSFs as a function of declination generated for a limiting dynamic range of 500 without any interpolation. From the plot we note that the difference is nearly uniform (variation from one end to another is 0.0016%). The total number of PSFs required for the entire declination range (-75° to -5°) is 240. Each PSF has a size of 513×513 pixels and occupies ≈1 MB of memory[8]. The memory required is quite a high number, but compared with the capacity of virtual memories available in the present day computers, it is a manageble requirement. In addition, since we deconvolve image covering only one delay zone (≈35°) at a time, the actual number of

[8]each value stored as float occupying four bytes.

PSFs loaded in the virtual memory would be lesser.

We define this non-uniform grid in declination (-75° to -5°) such that the maximum difference between the two consecutive PSFs on the grid is constant and is ≈0.4% as the *Master Declination Grid*. Since the images for different delay zones are deconvolved separately the total number of PSFs required would be larger due the overlapping region in declination. The total number of PSFs needed for each of the four delay zones (including the guard zones) are 30, 55, 115 and 200 respectively (for I, II, III and IV delay zone; see Table. 5.3). Thus the total number of PSFs required to deconvolve an image covering one sidereal hour range and all the four delay zones for a dynmaic range limitation of 500, is 400.

6.3.3.3 Optimizing the run time performance

Estimation of PSF is computationally expensive. Our approach involves a large number of PSFs on the Master declination grid which is very time consuming. Typically a full resolution PSF of size 513×513 pixels takes ≈40 minutes on a 2.4 GHz Intel PC. In order to compute the 400 PSFs to deconvolve an image corresponding to a given sidereal hour range and all the four delay zones, it would take ≈300 hours which is prohibitively large. The problem gets further aggravated if one discards a few of the each day images due to poor quality during co-addition and remakes the full resolution dirty image. In such a scenario all the PSFs would have to be estimated again. For each sidereal hour the PSFs have to be computed separately owing to different allocations used, different sources used to estimate the relative gains and bandwidth decorrelation. This scenario for estimation of PSFs based on this approach is prohibitive and impractical. On careful analysis of the entire process we noted the following.

- The major time in estimation of the PSF is spent on computing the trigonometric functions (*cosine* in our case).
- Within each day's image the aperture illumination is assumed to be uniform.
- The full resolution PSF at any declination is a weighted sum of the individual allocation's PSFs for any given declination.

Look-up PSFs of each allocation for full resolution look-up PSF: These hinted to the idea that if we assume the delay beam to be a step function (staircase like), in which the decorrelation within one allocation does not change significantly from baseline to baseline (as only stretch of 84 m along NS is covered in one allocation), we can assume one single value for the bandwidth decorrelation for any allocation (which is the average decorrelation suffered by all the baselines in that allocation at the concerned declination). In such a case

the full resolution PSF at any declination can be obtained by simply co-adding the PSFs of different allocations used, with appropriate relative weights to include the effect of bandwidth decorrelation. If the PSFs for each of the individual allocations is readily available at each declination on the Master declination grid, the computation of the full resolution PSF can be done significantly faster.

So for each allocation we would need 240 PSFs on the Master declination grid. In addition, the visibilities in the first 12 configurations have been measured with two slightly different sets of baselines and this makes the effective number of configurations to 75 ($\because$ 2*12+63=75). Thus the total number of PSFs needed for all the allocations is 240×75=18,000. The time required to compute a PSF of size 513×513 pixels for one allocation is ≈40 seconds ($\because$ No. of baselines is only 32×15 compared to 32×881 in the full resolution). Thus the total time required for all the PSFs to be generated would be ≈18000×$\frac{2}{3}$ minutes which is ≈10 days. The memory[9] required for storage of these PSFs on the hard drive would be ≈513×513×4×75×240 bytes≈18 GB. *It is to be noted that this exercise has to be carried out only once for the entire survey as it is independent of amplitude gain and bandwidth decorrelation.*

Fig. 6.12 shows the flow chart of the major steps involved to estimate the PSFs at each declination on the Master declination grid for all the allocations. These PSFs are stored on the hard drive and referred to as *Master PSF bank* and can be retrieved as and when needed while computing the full resolution PSF.

Estimation of the full resolution PSF :

The full resolution PSF at any declination is estimated by co-adding the retrieved individual allocation PSFs at that declination from the Master PSF bank with appropriate relative weights to take into account the effect of bandwidth decorrelation. Fig. 6.13 shows the steps involved in estimation of the full resolution PSF. It is to be noted that since the retrieval time of the PSF of an allocation(<<1 s) is significantly faster compared to its computing time (≈40 s), this approach has drastically reduced the time required for simulation of all the PSFs for one sidereal hour range and all the four delay zones to just ≈2 hours. This is dramatically less compared to ≈300 hrs in case of brute force computation by a factor of ≈150. Thus full resolution PSFs for deconvolving any sidereal hour image are generated using this approach before starting the deconvolution within very practical time limits.

The significant reduction in the time required in estimation of the PSFs also enables us to re-estimate them when the user discards images of a few allocations due to bad quality and remakes the full resolution image. For bright sources (using Eqn. 6.8), the PSFs are estimated separately by the normal method. The number of such sources are very few for

[9] each value stored as float occupying four bytes.

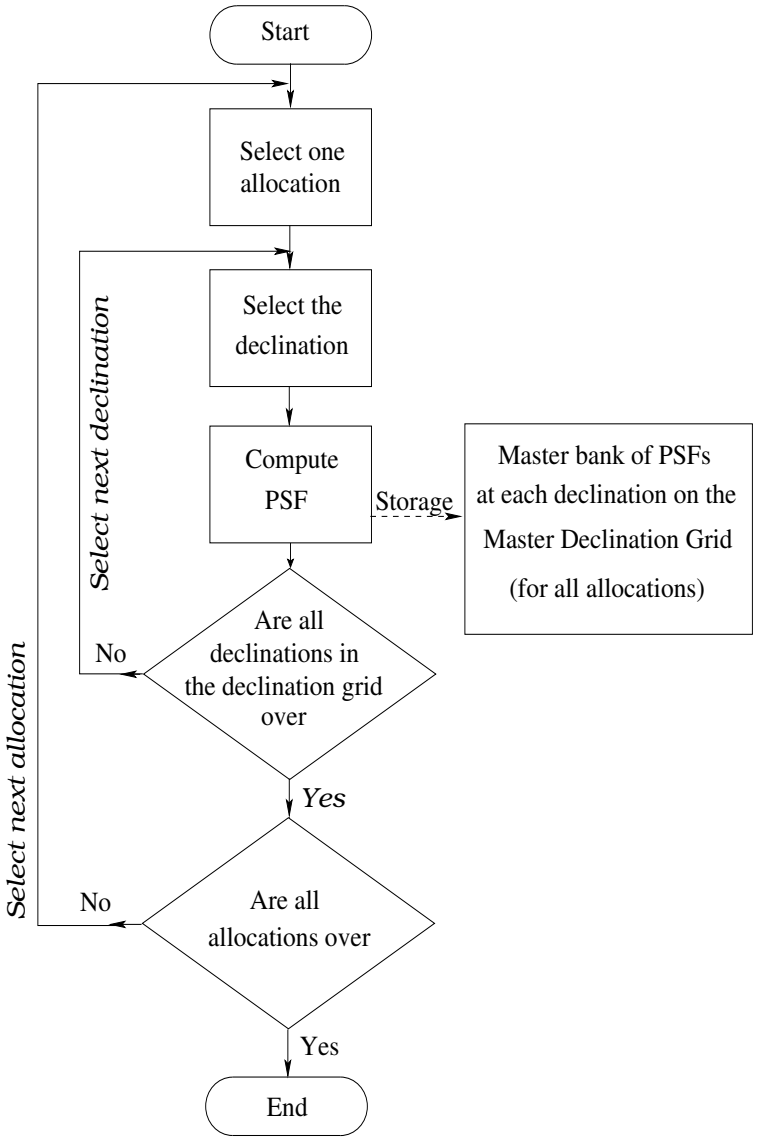

Fig. 6.12: The flow chart shows the steps involved to accomplish the master bank of PSFs at all declinations on the master declination grid for all the allocations. These PSFs are stored on a hard drive and retrieved as and when required to estimate the full resolution PSFs.

an image.

6.3.4 MRT CLEAN

The scheme developed to deconvolve the full resolution wide field dirty images taking into account the declination dependence of the PSF and other complexities is referred to as MRT CLEAN and is carried out interactively via a stand-alone GUI based program which uses Högbom CLEAN algorithm. Fig. 6.14 shows a snapshot of the GUI interface of the deconvolution program. The program is written in C and uses the *pgplot* graphics library. The GUI interface comprises of two windows containing the original dirty image and the

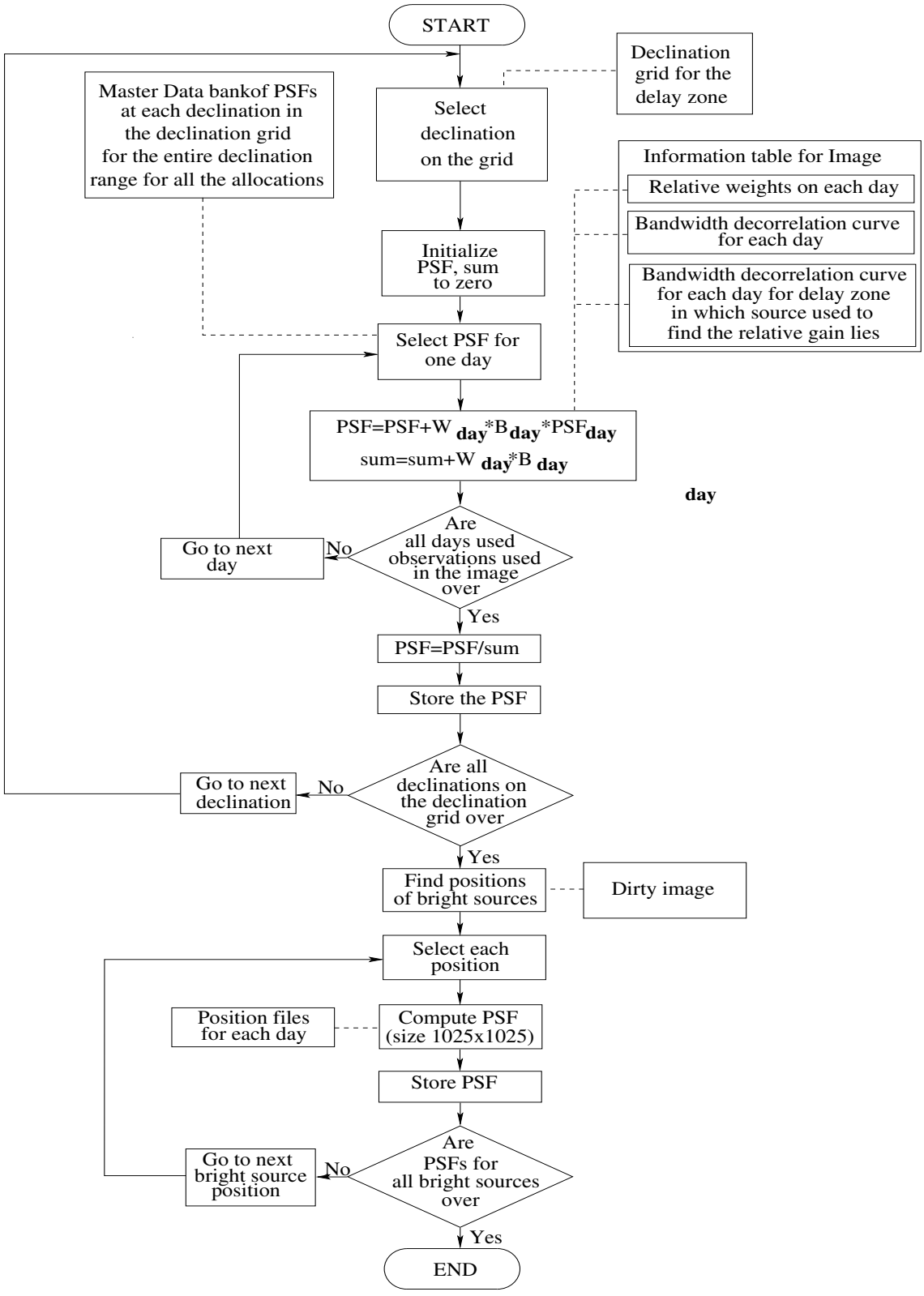

Fig. 6.13: Flow chart for the steps involved in estimation of full resolution PSF. The dashed line indicates the referral/retrieval of information already available, or being stored. W_{day} corresponds to the weights given to each day's image and B_{day} is the effective weighting changed due to bandwidth decorrelation at the concerned declination.

current residual image. At the start the residual image is same as the original dirty image and changes as CLEAN progresses. The GUI interface has provisions for zooming subparts, masking regions etc. but we will exclude a detailed discussion of the software aspects here.

The steps of deconvolution are shown in Fig. 6.15. At MRT the imaging is carried out on a sidereal hour basis. For each sidereal hour range, the images are produced separately for all the four delay zones. The dirty image as mentioned earlier is first convolved with a *sinc* function of resolution expected at declination δ=0° (16 s). This smoothens out any amplitude scintillations lasting shorter than 16 s and also helps to prevent the CLEAN procedure from oscillating. There is no smoothening done along the declination as it is the direction of synthesis.

For deconvolving the wide field images (40°×35°) corresponding to a given sidereal hour and a delay zone, we generate PSFs (extent ≈ 9°×15°) at specifically chosen declinations such that the maximum error by approximating the PSF at any declination with the closest available PSF is <0.2%. This approach has some similarities with the 'beam set' approach (Waldram & McGilchrist, 1990). Additionally, the positions of bright sources having flux densities above a threshold limit (Eqn. 6.8) are estimated from the raw images and PSFs (extent ≈ 18°×15°) are generated at those declinations. The generated PSFs are stored as a data bank on the hard drive. The deconvolution is carried out using Högbom CLEAN (Högbom, 1974) and the deconvolved image of interest has a size of ≈15°×15°. During the deconvolution the algorithm approximates the PSF at the current detected peak position by the closest available PSF. This avoids the need for PSF interpolation in the image plane at each iteration in the CLEAN loop. The important parameters like strength of the current peak and its position, rms noise, iteration number etc. are dynamically displayed after intervals which is decided by the user.

6.3.4.1 The use of boxes

In general to restrict the number of degrees of freedoms, the regions of image which are searched for the peaks is restricted to those areas (known as CLEAN boxes or windows) within which emission is known or guessed to be present. For a simple source, or a few sources, multiple boxes can be used in practice. Since, we are dealing with wide field images having a number of sources, it was practically difficult to mark such regions. Instead we masked such regions using the Graphical User Interface of the deconvolution program, which are not considered to be present due to real emission. We call such regions as forbidden boxes or windows. These masked (forbidden) regions are not searched for peaks during the CLEAN.

The main sources which complicated the deconvolution procedure are mentioned in

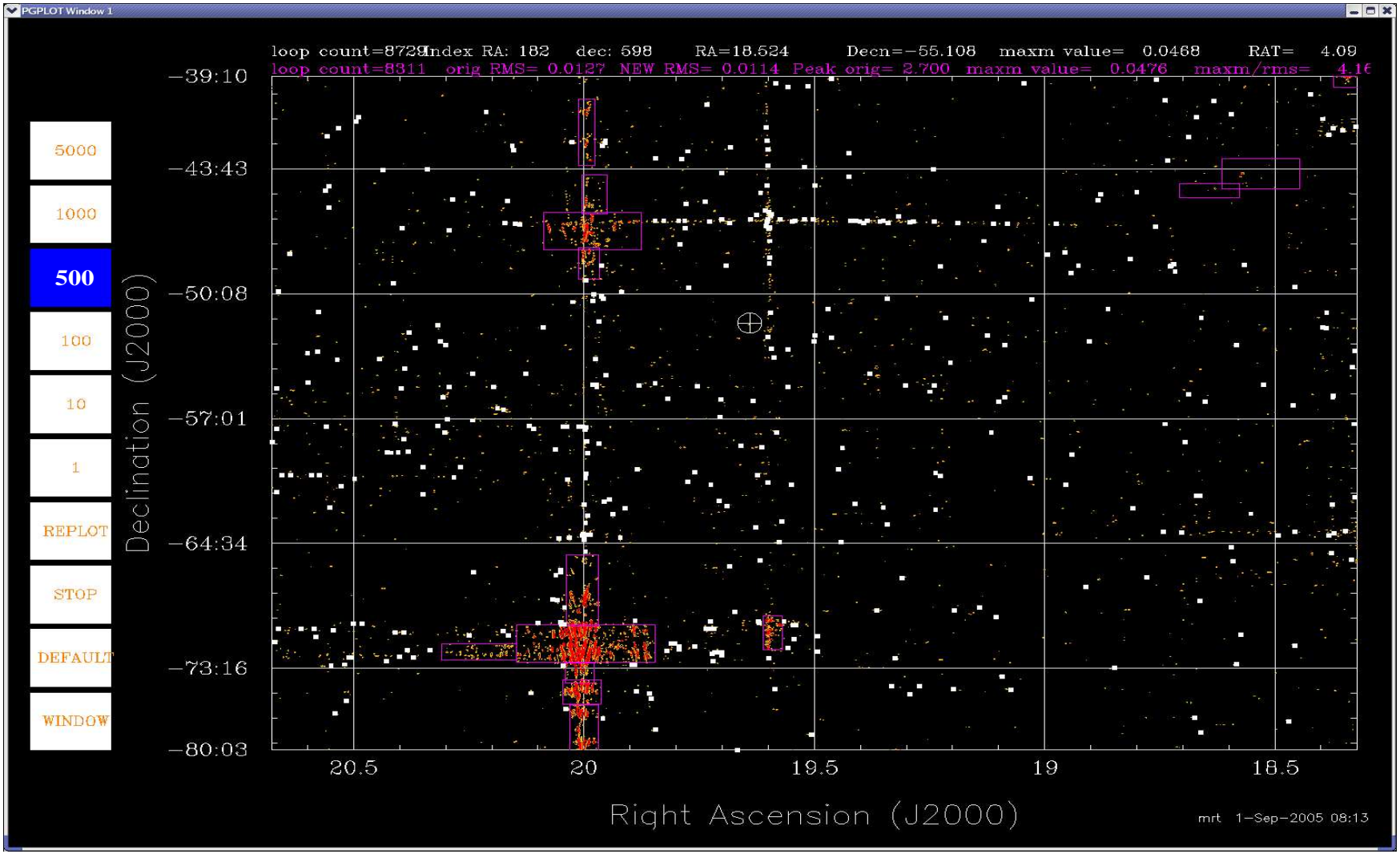

Fig. 6.14: A snapshot of the GUI interface of deconvolution program. The buttons shown on the left provide various options to carry out different functionalities in addition to various key based commands. The parameters as the CLEAN progresses are dynamically displayed on the top as shown. The rectangles in magenta show the regions which are suspected to have non-astronomical origin (or not of interest) and are masked as forbidden windows during the CLEAN. The small white filled squares show the locations where the clean components have been detected earlier in between the last halt (loop count 8311) and the present step (loop count 8729). The location of the current detected peak is shown by an encircled plus sign.

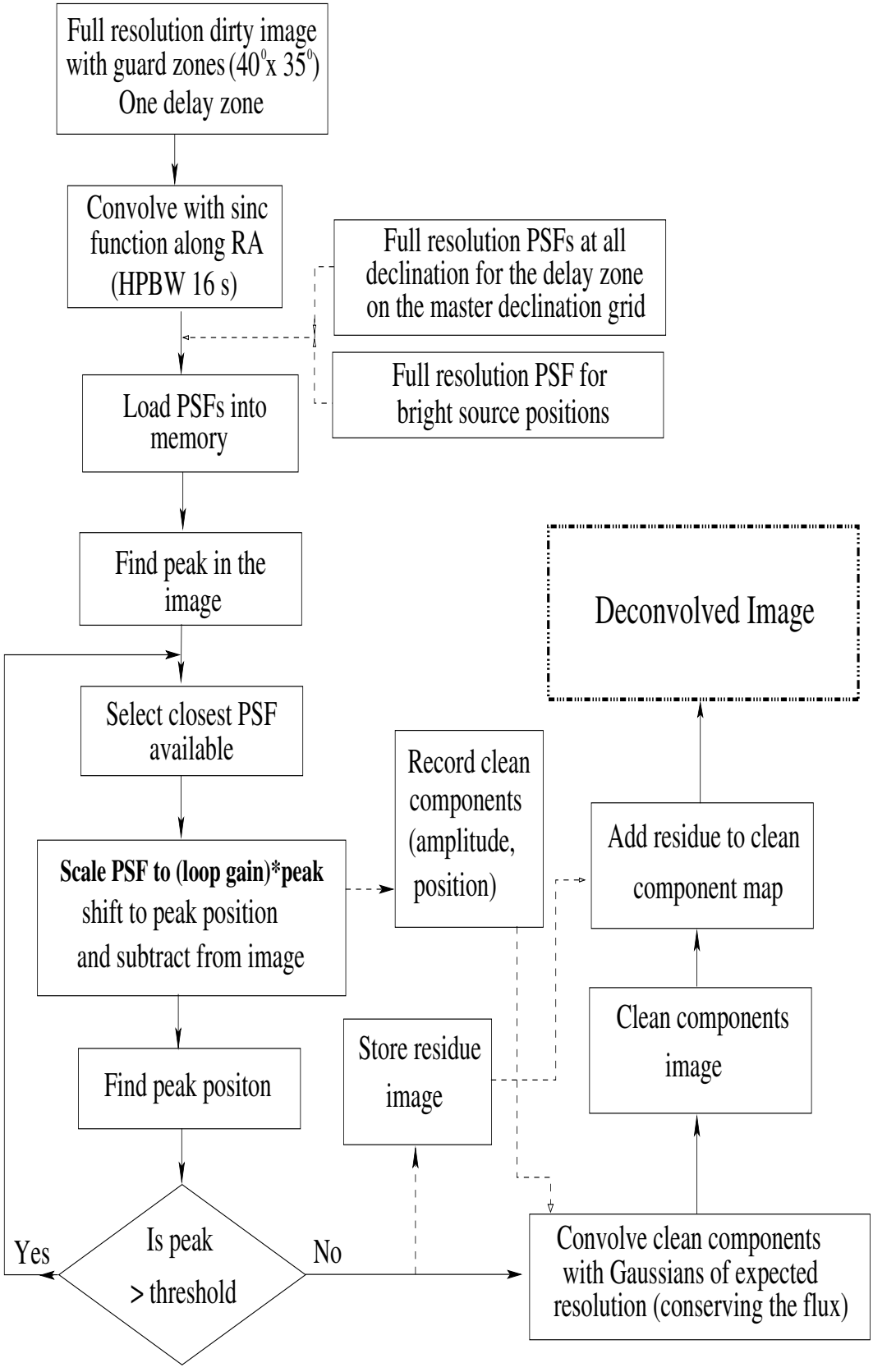

Fig. 6.15: Flow chart showing the steps involved in deconvolution. The dashed line indicates retrieval of the required information from earlier steps of data processing or being recorded.

Source Name	RA (J2000)	DEC (J2000)	Flux density (S)
Cas A (3C 461)	23:23:26	58:49:34	S_{159}=13,000 Jy
Cygnus A (3C 405)	19:59:29	40:44:16	S_{159}=8,600 Jy
MRC1932-464	19:35:57	-46:20:44	S_{150}=97 Jy
MRC2152-699*	21:57:06	-69:41:33	S_{150}=102 Jy
MRC2211-172	22:14:25	-17:01:44	S_{150}=93 Jy
MRC2356-611*	23:58:48	-60:53:00	S_{150}=170 Jy

Table 6.1: The sources which caused notable complications during deconvolution. The sources Cas A and Cygnus A appear as grating lobes in the images corrupting the entire declination range of MRT in the images. The other three sources appear as aliased images at multiple locations along declination at the true RA of these sources. The regions affected by the sources shown by $*$ are actually additionally corrupted due to 2 or 3 strong sources near them.

Table 6.1 (also see Fig. 7.29 for the extent of the regions affected by these sources). The most difficult regions to be dealt with were due to Cas A and Cygnus A in the northern sky which appear in grating lobes at multiple locations in declination and thus corrupt portions of image making them unusable. The aliased images due to source MRC2356-611 also appeared at multiple locations in declination, thus corrupting the image. The other two sources MRC2211-172 and MRC1932-464 also have aliased images at multiple locations, although of less strength. There are other strong sources also near MRC2152-699 which together corrupt comparatively a larger region. Few other sources although comparatively weaker posed some difficulties. In order to ensure that the spurious features do not destabilize the CLEAN, these were masked in the starting of the deconvolution program, but occasionally we needed to add masked regions during intermediate stages of CLEAN when such features were revealed.

At a few locations in the wide field images, it was difficult to make a good guess as to whether a particular feature was due to a genuine source or an artifact. This is arduous when the real emission regions have overlap with the spurious features. In order to minimize human errors in masking such regions we made use of the MRC catalogue at 408 MHz. Positions of all the sources listed in MRC in the region were superposed on the image whenever required. Owing to comparable resolution, sensitivity and nearby frequency of the MRC, this does comes as a rescue more often than not, for distinguishing such artifacts from genuine sources in doubtful cases.

6.3.4.2 CLEAN beam or restoring beam

The images were CLEANed down to a level of 5σ, where σ is the rms noise in the maps in the sidereal hour range of interest (and not in the guard zones). The rms fluctuations itself varies across the image from one region to the another with RA, due to the change in

the brightness temperature of the sky (discussed in the next chapter). Along declination at any given RA the rms noise is nearly constant. We used a loop gain (γ) of 0.05. The number of iterations required is generally between 15,000-25,000 depending upon the region to be CLEANed for a typical dirty image covering 40°×35°.

The CLEAN components were convolved with a two dimensional elliptical Gaussian in RA and $\sin(za)$ domain having a FWHM equal to the expected resolution ($4'\times4'.6\sec(\delta+20^\circ.14)$) corresponding to the maximum baseline observed. The bandwidth decorrelation changes the synthesized beam width in the dirty image along $\sin(za)$, at the expense of the amplitude, thus conserving the flux. The area of the normalized dirty beam and the normalized restoring beam at each declination is estimated and the convolving Gaussian is appropriately scaled while convolving the CLEAN components to ensure that the flux is appropriately restored. The area of the normalized Gaussian is higher than the normalized dirty beam, hence the corresponding heights of the convolving Gaussian were lower than unity (0.8-1.0). The residues are added to the map resulting from the convolution of the CLEAN components with the restoring beam to obtain the deconvolved map.

6.3.4.3 Dynamic range

The dynamic range is the ratio of the flux density of the weakest source and the strongest source in a given region which can be considered reliable. Clearly this will depend upon how close or far away one is from a strong source. In addition, in the present case it also depends upon the direction. In RA and declination directions the reduced sidelobes of a point source is ≈1.4% to 1.5% of the peak value. Thus the achieved dynamic range is ≈70. The dynamic range in the direction of the diagonals is higher. Fig. 6.16 shows the dirty image and the deconvolved image of the same region. The weak source MRC2248-411 (flux density ≈1 Jy at 408 MHz) which was buried in the sidelobes of MRC2250-412 (flux density ≈14 Jy at 408 MHz) in the dirty image can be easily seen in the deconvolved image.

6.3.5 Strengths and limitations of MRT CLEAN

Deconvolution of wide field image made with the non-coplanar array like MRT is an intricate task. The PSF varies across the declination, due to non-coplanarity of the array, bandwidth decorrelation and the variation of beam in RA as $\sec(\delta)$. The effect of each of these factors have been analysed and taken into account. The effects of precession and interference have been found to have negligible effect on the PSF and are ignored.

We have optimized the computational requirements by use of look-up PSFs first at the level of each day to estimate the full resolution images. The full resolution PSFs are again

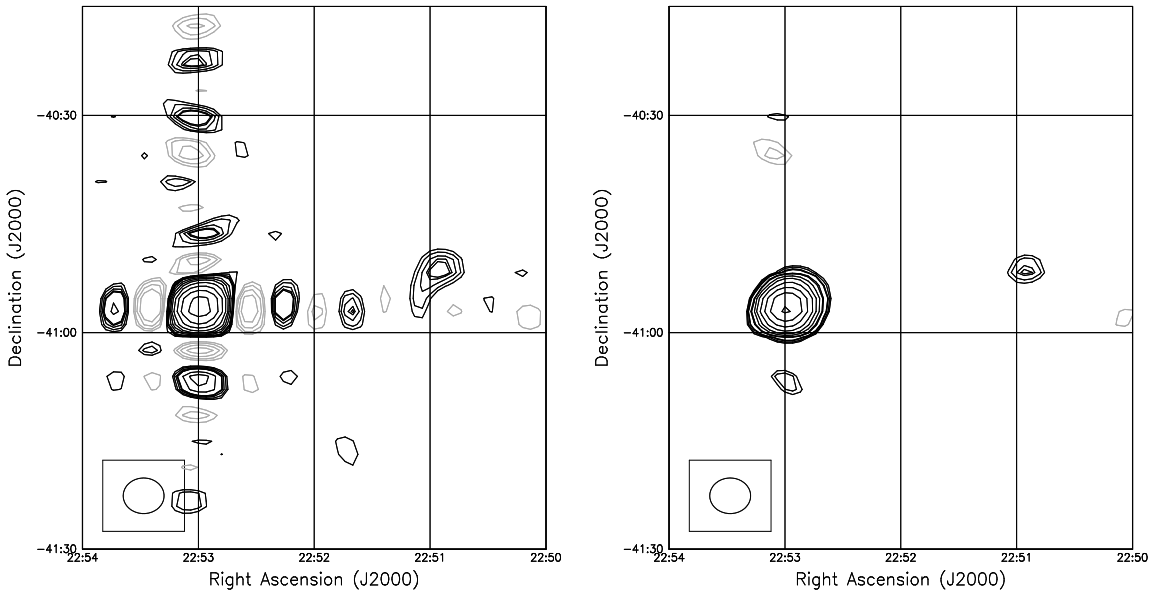

(a) Dirty image

(b) Deconvolved image.

Fig. 6.16: The plot shows (a) dirty and (b) deconvolved image of the same region at 151.5 MHz from MRT. The weak source MRC2248-411 (flux density ≈1 Jy at 408 MHz; 2.7 Jy at 151.5 MHz) which was buried in the sidelobes of MRC2250-412 (flux density ≈14 Jy at 408 MHz; 31 Jy at 151.5 MHz) in the dirty image can be easily seen in the deconvolved image. The contour levels are -2.8, -2.0,-1.4, 1, 1.4, 1.8, 2.5, 3.8, 6, 7, 10, 14.4, 20, 28.8, 40 Jy beam^{-1}.

used as look up tables during deconvolution. The estimation of minimum number of full resolution PSFs required for obtaining a given dynamic range by co-adding the already stored each allocation's PSF with appropriate weights, has dramatically decreased the time required for estimation of PSFs. Due to this it was practically feasible to generate a large number of PSFs which can be used to deconvolve the full resolution dirty images. In addition, for bright sources PSFs at their actual position in the image and of larger extent were estimated to ensure appropriate deconvolution. The PSFs for each allocation on the Master declination grid have to be generated only once for the entire survey as it is independent of amplitude gain and bandwidth decorrelation.

The method adopted by us has been motivated by the use of look-up tables in the computer science field. Earlier similar approach of using "Beam-Sets" has been reported by Waldram & McGilchrist (1990) mainly for source fitting and image analysis. It is important to mention that the problem of deconvolution is computationally more expensive compared with the source fitting, since the PSF is required at each iteration. Since, we use a loop gain of 0.05 it translates to a factor of ≈20 in terms of computation. Our scheme also does not require PSF interpolation during each iteration in the CLEAN loop.

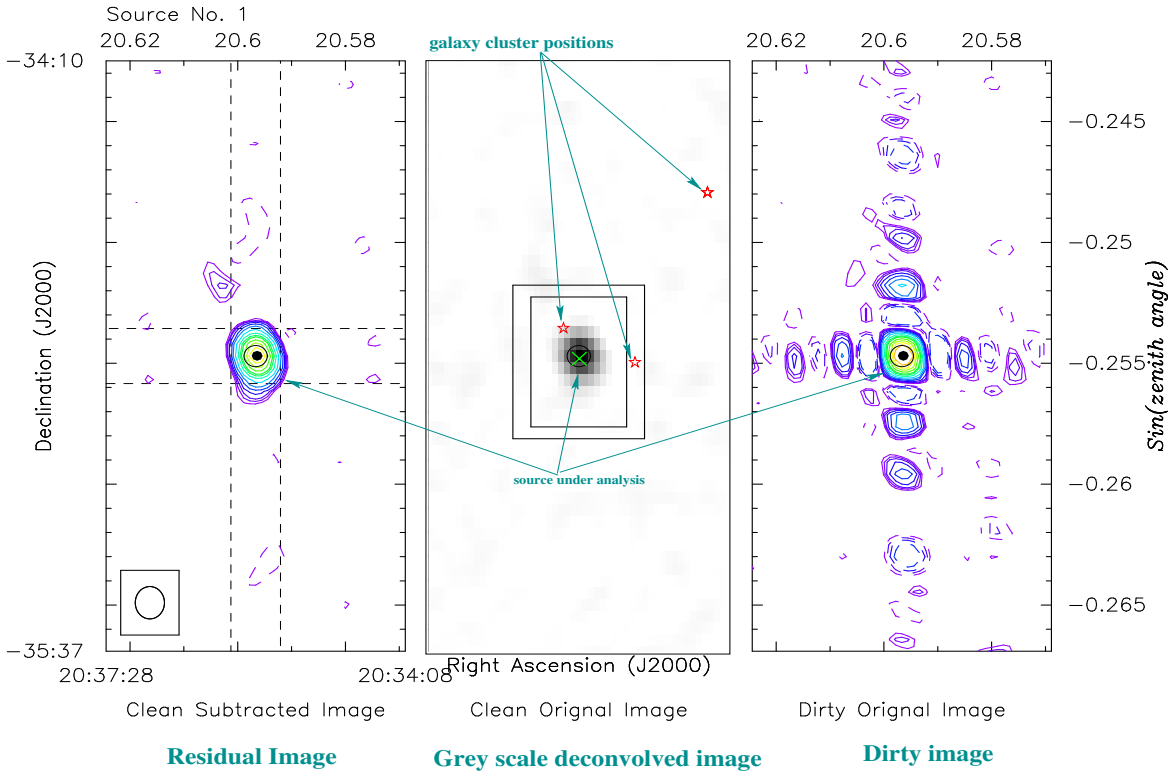

Fig. 6.17: The dirty and the deconvolved image of the source MRC2032-350 which has a flux density of ≈33 Jy (at 151.5 MHz). The contour plot on the extreme right shows the dirty image, the contour plot on the left and the grey scale image in the center show the deconvolved image of same region. The color bar shows the intensity scale in arbitrary units.

The required software was developed in-house to accomplish the above mentioned tasks. It has provision for masking regions, zooming and plotting the MRC sources to help in distinguishing genuine sources from the artifacts. In the first run, the location of all the sources whose strength is more than 0.7 times the peak in the dirty image is noted down and only those PSFs are loaded in virtual memory. Thereafter as and when required, the PSFs are automatically loaded into virtual memory. This makes sure that even for computers with modest virtual memory, a sufficient part of the deconvolution is run without overloading the memory of the system. The noise is calculated in intervals of few hundred iterations which is decided dynamically by the rate at which the noise decreases as the CLEAN progresses and the peak in the residual image approaches close to 5σ. This also decreases the computational requirements during CLEAN.

We have not deconvolved the regions covering the Galactic plane (RA range 15:06 hrs to 18:00 hrs and declination range -75° to -10°). Initial attempts to deconvolve revealed creation of well known artifacts in the form of stripes. In our method we search for absolute maxima since generally the background is non-varying. This may not be the best pro-

cedure for regions covering the Galactic plane. In case of varying large scale background, instead of the absolute maxima an alternative approach is to search for local maxima. This was proposed and successfully employed to deconvolve the entire image of GEETEE survey including the Galactic plane (Dwarakanath, Deshpande, & Udaya Shankar, 1990). It is to be noted that the same approach can also be easily attempted without any major change in the entire deconvolution procedure. The software developed can be fully used as such, except for changing the maximum finding function. Due to limitation of time this was not carried out for this dissertation. Alternatively, one may employ algorithms like Multi Resolution Clean, Wavelet CLEAN, or the MEM. At this stage it is not clear which one of these would be finally employed.

The full resolution dirty images covering more than one steradian of the sky were successfully deconvolved to obtain deconvolved images covering the RA range 18 hrs to 24h39m and declination range -75° to -10° using the procedure developed. Fig. 6.17 shows the dirty and the deconvolved image of the source MRC2032-350 which has a flux density of ≈33 Jy at 151.5 MHz. Fig. 6.18 shows the wide field dirty image covering RA range 20 hrs to 21 hrs and the declination range -60° to-50°. The corresponding deconvolved image is also shown in Fig. 6.19. The deconvolved images presented here and in the next chapter demonstrate the success of the method developed.

The deconvolved images for each sidereal hour range are in arbitrary units and not on the same scale. Further analysis of deconvolved images related to flux calibration and catalogue construction is discussed in Chapter 7. Subsequently they are also presented as a set of contour maps.

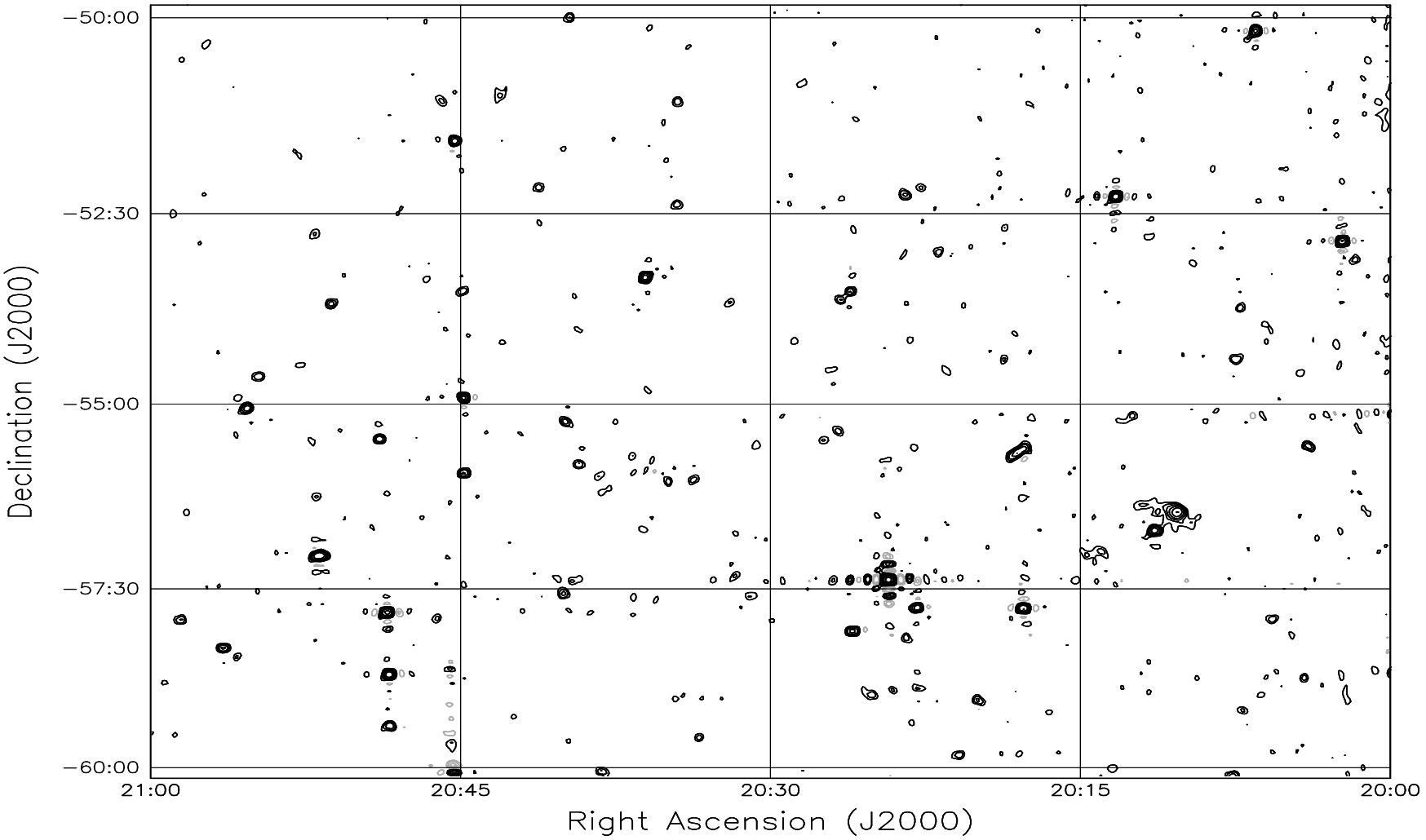

Fig. 6.18: The full resolution dirty image of a region covering RA range 20 hrs to 21 hrs and declination range -60° to-50°. The resolution of the image shown is 7′×5.′6. The contour levels are 3, 5, 7, 10, 14, 20, 28, 40, 60, 100×σ where σ is the rms noise in the image. The image intensity is in arbitrary units. The deconvolved image of the same region is shown in Fig. 6.19.

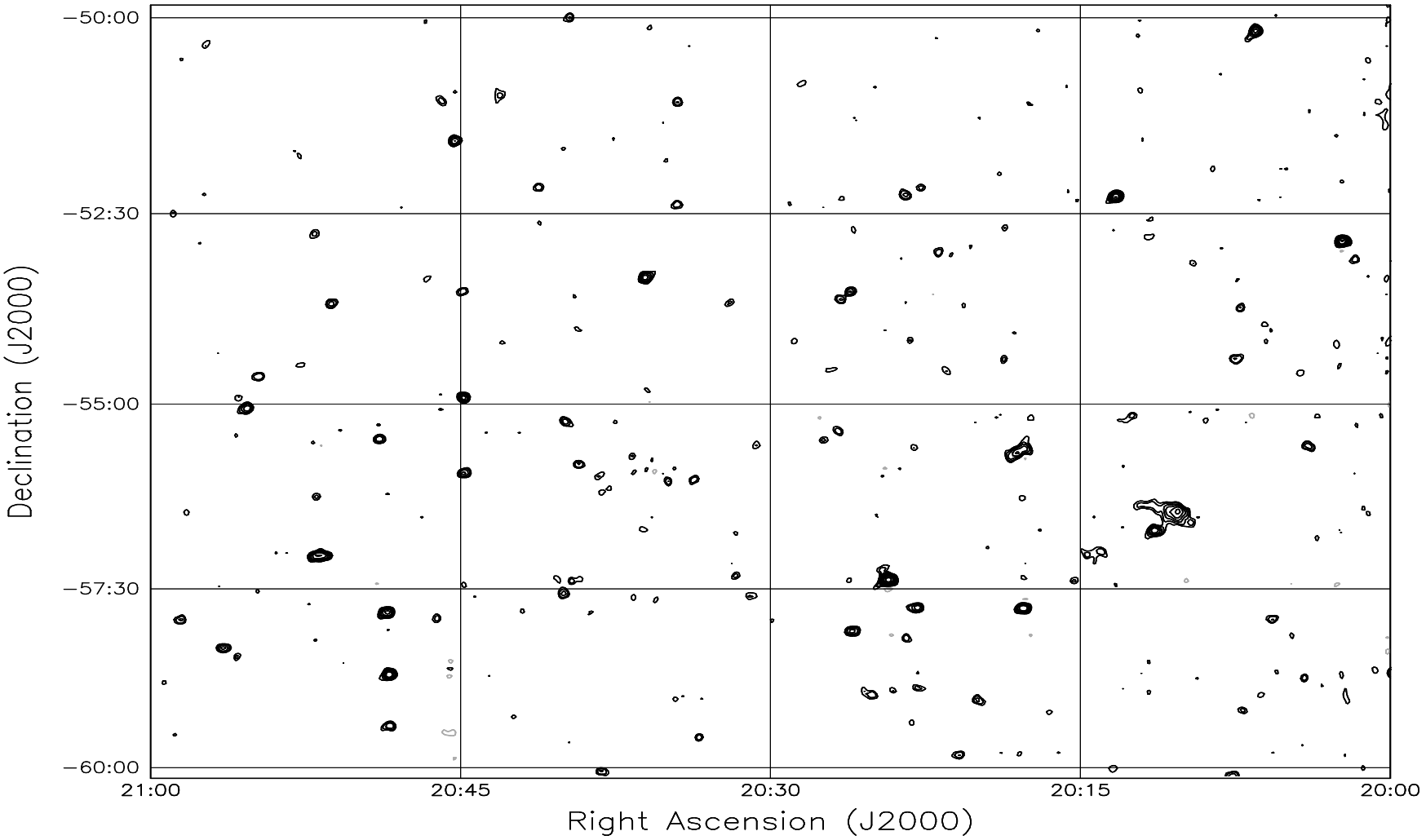

Fig. 6.19: The full resolution deconvolved image of a region covering RA range 20 hrs to 21 hrs and declination range -60° to-50°. The resolution of the image shown is 7′×5.′6. The contour levels are 3, 5, 7, 10, 14, 20, 28, 40, 60, 100×σ where σ is the rms noise in the image. The image intensity is in arbitrary units. The dirty image of the same region is shown in Fig. 6.18.